

Experimental Progress in Thermal Hall Conductivity Research on Strongly Correlated Electronic Systems

XU Hao¹, CHENG Shu-fan¹, BAO Song^{1*}, WEN Jin-sheng^{1,2†}

1. National Laboratory of Solid State Microstructures & Department of Physics, Nanjing University, Nanjing 210093, China

2. Collaborative Innovation Center of Advanced Microstructures, Nanjing University, Nanjing 210093, China

Abstract: Thermal Hall effect (THE) is to describe the phenomenon where heat carriers are deflected by an external magnetic field applied perpendicular to the heat flow, and thus the carriers gain transverse velocity, leading to a finite temperature gradient on the two sides orthogonal to the heat flow and field. THE is predicted to occur in systems with nontrivial Berry curvatures and thus can reveal topological properties, similar to the electrical Hall effect. However, THE is not limited to charge excitations as in the electrical Hall effect, but rather, to all kinds of excitations that are able to conduct heat, making it possible to explore the exotic properties in strongly correlated electronic systems, which are typically insulators. Therefore, THE is more universal than the electrical form and has become a powerful probe in detecting charge-neutral excitations, such as phonons and magnons. Moreover, there are some sources such as chiral phonons, which are beyond a simple nontrivial-Berry-curvature scenario, that can also give rise to THE; examining THE wherein will shed light on the complex microscopic mechanism hidden in materials. Despite these, heat signals are much weaker than electrical ones. Especially for measurements of the thermal Hall conductivity, it is often needed to collect weak signals on top of a large background. This makes measuring the THE challenging—but thanks to the sustained efforts of the community, this field is developing rapidly in recent years, with many interesting results on the measurements of the thermal Hall conductivity. In this review article, we try to summarize some of these exciting accomplishments, point out remaining outstanding issues, and suggest possible future directions.

Key words: thermal Hall effect; topology; quantum spin liquid; multiferroics; pseudogap phase

CLC number: O469 **Document code:** A **DOI:** 10.13725/j.cnki.pip.2022.05.001

CONTENTS

I. Introduction	160	3. Perovskite Oxides	165
A. Background	161	B. Phonon Hall Effect	167
1. Fourier's Law	161	C. Materials with Controversial Origins of THE	168
2. Onsager's Rule	161	1. α -RuCl ₃	168
B. Measurements	161	2. Multiferroics (Fe _{1-x} Zn _x) ₂ Mo ₃ O ₈	174
II. THE in Strongly Correlated Electronic Materials	162	3. Cuprate High-Temperature Superconductors	175
A. Magnon Hall Effect Induced by DMI	162	III. Conclusion and Outlook	176
1. Lu ₂ V ₂ O ₇	163		
2. Cu(1,3-bdc)	164		
		Acknowledgments	179
		References	179

Received date: 2022-8-25

* E-mail: songbao@nju.edu.cn

† E-mail: jwen@nju.edu.cn

I. INTRODUCTION

The ordinary Hall effect in conductors is caused by the transverse Lorentz force acting on free electrons when a perpendicular magnetic field is applied. The magnetic field and the Lorentz force play an essential role here to deflect the electrons. However, with the discovery and explanation of quantum Hall effect^[1–3] and fractional quantum Hall effect^[4–6], the nonzero Berry curvature Ω has been considered as the root cause of the transverse velocity and the magnetic field is just one of the approaches to generate the transverse component, which is especially true in real crystalline materials when carriers are treated as quasiparticles. In the topological band theory^[7–13], quasiparticles can gain transverse velocity from nonzero Berry curvature, highly similar to the electrons gaining transverse velocity due to the Lorentz force. The overall effect, the Hall conductivity, is determined by the integral of the Berry curvature of the energy band over the occupied Brillouin zone. In some ferromagnetic materials, with the help of spontaneous magnetization, the Berry curvature can be nonzero even when a perpendicular magnetic field is absent, and the Hall conductivity can be nonzero (anomalous Hall effect^[14,15]) or even quantized (quantized anomalous Hall effect^[16]) without a magnetic field, suggesting again the close relationship between the Berry curvature and the Hall conductivity. Importantly, the Berry curvature is intricate to the wavefunctions of the energy bands, nothing to do with the constituent quasiparticles. Thus it is plausible that spins, as well as charge-neutral excitations such as magnons and phonons, can also result in the Hall effect as long as their energy bands are with nontrivial Berry curvatures^[17–20]. For spins, there are spin Hall effect^[21–23] and quantum spin Hall effect^[9,24–26]. For magnons and phonons, since they are both heat carriers, such a process can result in a “thermal Hall effect” (THE), which describes the generation of a finite temperature gradient on the two sides of the material along the direction orthogonal to the applied heat current and magnetic field, analogous to the electrical Hall effect. THE is originally considered to occur in conductors where electrons are dominant heat carriers. In that case, THE is simply caused by Lorentz force, just the

same as the Hall effect. It is a repetitive phenomenon and the explanation is a little trivial. Involved with topological band structure, however, THE is predicted to occur even in insulators and that is the attractive and interesting point. Therefore, in our discussions, “THE” is actually referred to that in insulators. Note that although the magnetic field does not generate the Lorentz force for THE, a field perpendicular to the heat current is still needed, in analogy to the electrical Hall effect. This will be discussed in detail later. Likewise, an anomalous THE version can also occur, which does not require the application of an external field^[27]. As such, THE greatly expands the range of transport measurements from electrical to thermal form, which is in principle applicable to any quasiparticle carrying thermal energy. It is particularly helpful in unveiling the exotic properties of strongly correlated electronic systems, which are mostly Mott insulators with frozen charge degrees of freedom, difficult for electrical transports to access^[28,29].

There are various models to generate nontrivial Berry curvatures that can be responsible for THE. For example, models with spin-spin interaction—Dzyaloshinskii-Moriya interaction^[28,30–34] (DMI), spin-lattice coupling^[35–37] or simply ionic bonding^[38] are suggested to explain or predict THE. Apart from these, other factors beyond Berry curvatures can also lead to a finite or even huge THE, such as skew scattering^[39,40], where scattering is much enhanced by antiferrodistortive transition, and chiral phonons as suggested in cuprates^[41]. As a consequence, THE opens a door for exploring materials concerning magnetic interactions and spin-phonon interactions. It also provides a probe to detect exotic charge-neutral excitations like Majorana fermions and to reveal the mystery microscopic mechanism through which we can further understand the nature of various unusual properties in materials.

Despite the many advantages of THE, measurements of the thermal Hall conductivity have been challenging due to the weak THE. It is required substantial efforts to enhance the weak THE response while maintaining a low background level. Due to the weak signals, many extrinsic factors such as the sample quality, contacts, and environmental noise can have signif-

ificant impacts on the measurement results. Nevertheless, a lot of fascinating experimental progress on THE in strongly correlated electronic systems has been made in recent years, providing many insights into the quantum physics underlying these materials. This review aims at reflecting on some of the interesting developments of the THE experiments.

The rest of the paper is organized as follows. In Sec. I., we introduce the background knowledge including the law of heat conduction (also known as Fourier's Law), Onsager's rule, and some measurement methods. In Sec. II., we discuss thermal Hall transport observed in DMI systems, pure phonon systems, and in the materials such as α -RuCl₃, multiferroics, and superconductors, where the origin of the thermal Hall conductivity is still under debate. In Sec. III., we make a brief conclusion of the review and provide some perspectives for future research.

A. Background

1. Fourier's Law

Analogous to the electrical case which is defined by Ohm's Law, thermal conductivity is defined by Fourier's Law.

$$\begin{cases} \mathbf{j} = \sigma \mathbf{E} & \text{Ohm's Law,} \\ \mathbf{q} = -\kappa \nabla T & \text{Fourier's Law.} \end{cases} \quad (1)$$

In Ohm's Law, \mathbf{j} , σ , and \mathbf{E} represent electrical current density, conductivity, and electric field, respectively, while in Fourier's Law, \mathbf{q} , κ , and ∇T are the heat flux, thermal conductivity, and temperature gradient, respectively. Generally, σ and κ are matrices because of anisotropy. The inverse matrix of κ is defined as the thermal resistivity matrix, ρ . If we only consider two dimensions:

$$\begin{pmatrix} q_x \\ q_y \end{pmatrix} = - \begin{pmatrix} \kappa_{xx} & \kappa_{xy} \\ \kappa_{yx} & \kappa_{yy} \end{pmatrix} \begin{pmatrix} \partial_x T \\ \partial_y T \end{pmatrix}, \quad (2)$$

where κ_{xy} is the thermal Hall conductivity.

2. Onsager's Rule

Onsager's Rule^[42,43] reveals the microscopic time-reversal symmetry. As shown in Eq. 2, even though we

only consider two dimensions, we have four independent coefficients unsettled. Onsager's Rule points out that when choosing the correct thermodynamic force \mathbf{X} and flux \mathbf{J} ^[43], the linear response coefficients confirm $L_{ij}(H) = L_{ji}(-H)$. That means in zero fields, the coefficients must be symmetric with $L_{ij} = L_{ji}$ while the antisymmetric terms can occur only when a magnetic field is applied. For heat flow \mathbf{q} , the corresponding thermodynamic force could be ∇T or $\nabla \frac{1}{T}$. The former is usually taken for convenience.

B. Measurements

Fig. 1 shows the schematic of the measuring apparatus, where there is a heater providing heat flow and a heat bath which is usually Copper or LiF in order to avoid the thermal Hall background, for the thermal Hall conductivity in these two materials is substantially zero. Applying a perpendicular magnetic field H , the misalignment of the thermometers T_B and T_C can be eliminated by using

$$\Delta T_{BC} = \frac{1}{2} [\Delta T(H) - \Delta T(-H)], \quad (3)$$

when the temperature gradient ΔT caused by the misalignment is field symmetric. When the longitudinal signal is hysteretic, we need to use

$$\Delta T_{BC} = \frac{1}{2} [\Delta T(H) - \Delta^* T(-H)] \quad (4)$$

instead^[44], where $\Delta^* T$ means H changes in an opposite direction compared to ΔT . For example, if ΔT is measured with H sweeping from negative to positive, then $\Delta^* T$ should be sweeping from positive to negative.

In most cases, when applying a heat flow in x -axis ($q_y = 0$), $|\partial_x T|$ ought to be much larger than $|\partial_y T|$. Additionally, in order to obtain κ_{xx} and κ_{xy} simultaneously in one measurement, we assume that $\kappa_{xx} = \kappa_{yy}$, and $\kappa_{xy} = -\kappa_{yx}$. Thus the thermal conductivity can be calculated using Eqs. 5 and 6, deduced from Eq. 2:

$$\kappa_{xx} = - \frac{q_x \partial_x T}{(\partial_x T)^2 + (\partial_y T)^2} \approx - \frac{q_x}{\partial_x T}, \quad (5)$$

and

$$\kappa_{xy} = - \frac{q_x \partial_y T}{(\partial_x T)^2 + (\partial_y T)^2} \approx - \frac{q_x \partial_y T}{(\partial_x T)^2} \approx - \frac{\kappa_{xx}^2 \partial_y T}{q_x}. \quad (6)$$

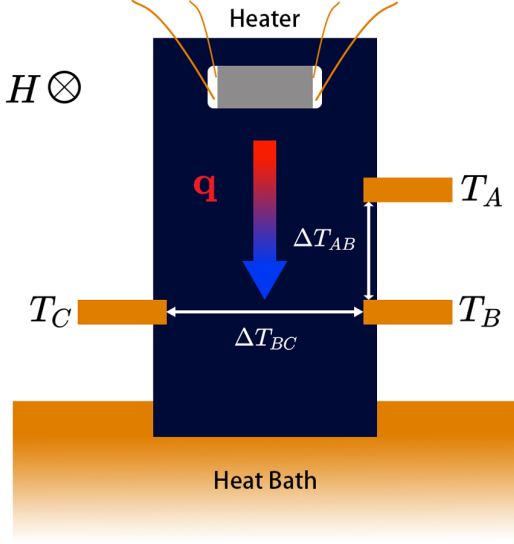


Fig. 1. Schematic of the apparatus for the thermal Hall conductivity measurements. T_A , T_B , and T_C denote the temperature read from the corresponding thermometers. \mathbf{q} and H are the heat current and magnetic field applied, respectively.

We note that in the formulas above, it is assumed that the thermal conductivity is isotropic in the plane. In the case where there is an in-plane anisotropy but the anisotropy is not so strong, like $\kappa_{yy} \approx \alpha \kappa_{xx}$ (α is close to 1)^[45], we can also get similar results with $\kappa_{xx} = -q_x/\partial_x T$, and $\kappa_{xy} = -\alpha \kappa_{xx}^2 \partial_y T/q_x$. It should be noted that $\kappa_{xx} \approx -q_x/\partial_x T$ works for most cases as long as $|\partial_x T| \gg |\partial_y T|$ and κ_{xy} is not extremely larger than κ_{xx} , analogous to the Ohm's Law $R_{xx} = U_x/I_x$.

The constraint $\kappa_{xy} = -\kappa_{yx}$ is typically used for three reasons. First, note that the off-diagonal term κ_{xy} can be decomposed into two parts, the symmetric part S_{xy} and the antisymmetric part A_{xy} , where $S_{xy} = \frac{1}{2}(\kappa_{xy} + \kappa_{yx})$ and $A_{xy} = \frac{1}{2}(\kappa_{xy} - \kappa_{yx})$. On the one hand, the antisymmetric part is independent of the selection of the coordinate system (which can be easily understood by the Group Theory), and thus it can reflect the intrinsic properties in materials (such as the Berry curvature), which are also nothing to do with the selection of the coordinate system. If we simply assume that there is only an antisymmetric term, then we can obtain the relation $\kappa_{xy} = -\kappa_{yx}$. On the other hand, according to Onsager's rule, the antisymmetric term can also reflect the time-reversal-odd scattering process, wherein $\kappa_{xy}(-H) = -\kappa_{xy}(H)$. Therefore, the

constraint is applicable for the two cases mentioned above, which are at the same time the major research subjects in recent years. Second, since the symmetric part is coordinate-dependent, it is feasible to reduce the symmetric part to the greatest extent by selecting the high-symmetry directions to be the x/y -axis. Third, the type of dominant Hall transport process could be actually detected experimentally. According to Eq. 2 (when $q_y = 0$), $\partial_y T \approx \Delta T_{BC}/d = \kappa_{yx} q_x/\mathcal{D}$, where d and \mathcal{D} are the distance between the two contacts and the determinant of the thermal conductivity matrix, respectively. Through Onsager's Rule it is easy to prove that \mathcal{D} is symmetric with the magnetic field, and thus if $\Delta T_{BC}(H) = \pm \Delta T_{BC}(-H)$, then $\kappa_{yx}(H) = \pm \kappa_{yx}(-H)$ which means the symmetric/antisymmetric term dominates. Therefore, if the symmetric term is dominant, $\kappa_{xy} = \alpha \kappa_{xx}^2 \partial_y T/q_x$ and if the system does not have any symmetry, measurements by two times (once $\mathbf{q} \parallel x$ and once $\mathbf{q} \parallel y$) are needed to determine the three or four coefficients.

For two-dimensional materials ($\kappa_{zi} = \kappa_{iz} = 0$, $i = x, y, z$), Eqs. 5 and 6 and the measuring methods are undoubtedly correct, but for the three-dimensional materials the difference between the two cases needs to be considered. The numerical difference must be small in order to make sure Eqs. 5 and 6 still work. For instance, when only considering $\kappa_{ij} = -\kappa_{ji}$,

$$\Delta = -\frac{q_x}{\partial_x T} - \kappa_{xx} = \frac{k_{xz}^2 k_{yy} + k_{xy}^2 k_{zz}}{k_{yz}^2 + k_{yy} k_{zz}}, \quad (7)$$

and therefore high-symmetry axis is preferred to be chosen as the $x/y/z$ -axis so that the diagonal terms are much larger than the off-diagonal terms, making the difference Δ negligible. After discussing some basic knowledge about thermal Hall conductivity, we will next show some measurement results of THE on some strongly correlated electronic systems.

II. THE IN STRONGLY CORRELATED ELECTRONIC MATERIALS

A. Magnon Hall Effect Induced by DMI

Dzyaloshinskii-Moriya interaction (DMI) (Eq. 8) is a type of antisymmetric spin coupling firstly sug-

gested by Dzyaloshinskii purely from symmetry perspectives in order to explain weak ferromagnetism of mainly antiferromagnetic crystals, such as α -Fe₂O₃^[30]. Moriya further suggested the explicit form of the “DM vector” \mathbf{D}_{ij} (Eq. 9) and Moriya’s Law^[31]. Later on, Fert and Levy^[32] suggested the Ruderman-Kittel-Kasuya-Yosida (RKKY) interaction of the DM type (Eq. 10). Moriya’s Law and Eq. 10 both point out the direction of the DM vector.

$$H_{\text{DM}} = \sum_{i,j} \mathbf{D}_{ij} \cdot (\mathbf{S}_i \times \mathbf{S}_j). \quad (8)$$

$$\begin{aligned} \mathbf{D}_{RR'}^{\text{ex}} = 2i\lambda \left(\sum_m \frac{\mathbf{1}_{mn}(R)}{\epsilon_m(R) - \epsilon_n(R)} J_{RR'}(nn'mn') \right. \\ \left. - \sum_{m'} \frac{\mathbf{1}_{m'n'}(R')}{\epsilon_{m'}(R') - \epsilon_{n'}(R')} J_{RR'}(nn'nm') \right), \quad (9) \\ J_{RR'}(nn'mm') = \iint \varphi_n^*(r_1 - R) \varphi_{n'}^*(r_2 - R') \frac{e^3}{r_{22}} \\ \varphi_m(r_2 - R) \varphi_{m'}(r_1 - R') dr_1 dr_2. \end{aligned}$$

$$\begin{aligned} H_{\text{DM}} = -V(\xi) \sin[k_F(R_A + R_B + R_{AB}) + \eta] \\ \left(\hat{\vec{R}}_A \cdot \hat{\vec{R}}_B \right) \frac{\left(\hat{\vec{R}}_A \times \hat{\vec{R}}_B \right) \cdot \left(\vec{S}_A \times \vec{S}_B \right)}{R_A R_B R_{AB}}. \quad (10) \end{aligned}$$

The magnon Hall Effect induced by DMI is closely related to the geometry and symmetry of the system. The DMI acting on the magnons or spin waves is just like a gauge field, providing a phase when magnons flow in the lattice^[33]. Moreover, the phase is only determined by $\mathbf{D}_{ij} \cdot \mathbf{n}$, where \mathbf{n} is the orientation of the spins and the indexes refer to the sites of the magnetic ions. Thus, it is obvious that how the spins are displaced and oriented in the lattice plays an important role here.

In recent studies, it is discovered that the DMI induced thermal Hall effect appears in perovskite oxides ABO₃^[33] and those with kagome lattice^[34,46] such as pyrochlore oxides A₂B₂O₇^[28,33]. They are all ferromagnetic insulators. By the way, it can be proved that the ferromagnetic ground state is stable against the DMI as long as $\sum_i \mathbf{D}_{ij} = 0$ ^[33].

Proof:

$$\begin{aligned} H_{\text{DM}} & \xrightarrow{\mathbf{S} \rightarrow \langle \mathbf{S} \rangle + \delta \mathbf{S}} \sum_{ij} \mathbf{D}_{ij} \cdot [\langle \mathbf{S} \rangle + \delta \mathbf{S}_i] \times [\langle \mathbf{S} \rangle + \delta \mathbf{S}_j] \\ & = \sum_{ij} \mathbf{D}_{ij} \cdot (\delta \mathbf{S}_i - \delta \mathbf{S}_j) \times \langle \mathbf{S} \rangle + o(\delta \mathbf{S}^2) = 0 \end{aligned}$$

1. Lu₂V₂O₇

One of the typical materials that exhibit the magnon Hall effect induced by DMI is Lu₂V₂O₇. The first observation and the successful theoretical explanation soon attracted intense attention and set off a series of research on this subject^[28]. The vanadium sublattice structure can be viewed as a stacking of alternating kagome and triangular lattices along the [111] direction. With the kagome lattice, nonzero DM vectors are predicted to occur. The lattice structure and the direction of DM vector are both shown in Fig. 2(a).

The κ_{xy} of Lu₂V₂O₇ as a function of the magnetic field at different temperatures is shown in Fig. 2(b). It becomes nonzero below $T_c = 70$ K and reaches the maximum when $T = 50$ K. As the temperature decreases, κ_{xy} gets smaller and finally disappears below 10 K. Besides these, one key feature is that κ_{xy} decreases as the magnetic field increases after a threshold field, which is evident at 50 K and below. Since Lu₂V₂O₇ is an insulator, the heat carriers can only be phonons or spins. If phonons dominate the conduction of heat, κ_{xy} ought to increase with the field because the fluctuation of spins reduces, resulting in a longer mean free path of phonons due to the weakening of scattering from spin fluctuations. The magnon scenario, where the population of magnons decreases as the magnetic field increases, appears to be more consistent with the observation of the decline of the thermal Hall conductivity.

Moreover, theoretical calculations based on this scenario, as is shown in Fig. 2(c), agree with the experimental data very well. The theoretical formula^[28],

$$\begin{aligned} \kappa_{\alpha\beta}(H, T) = \Phi_{\alpha\beta} \frac{k_B^2 T}{\pi^{3/2} \hbar a} \left(2 + \frac{g\mu_B H}{2JS} \right)^2 \\ \times \sqrt{\frac{k_B T}{2JS}} \text{Li}_{5/2} \left[\exp \left(-\frac{g\mu_B H}{k_B T} \right) \right], \quad (11) \end{aligned}$$

is derived from the Thouless-Kohmoto-Nightingale-den

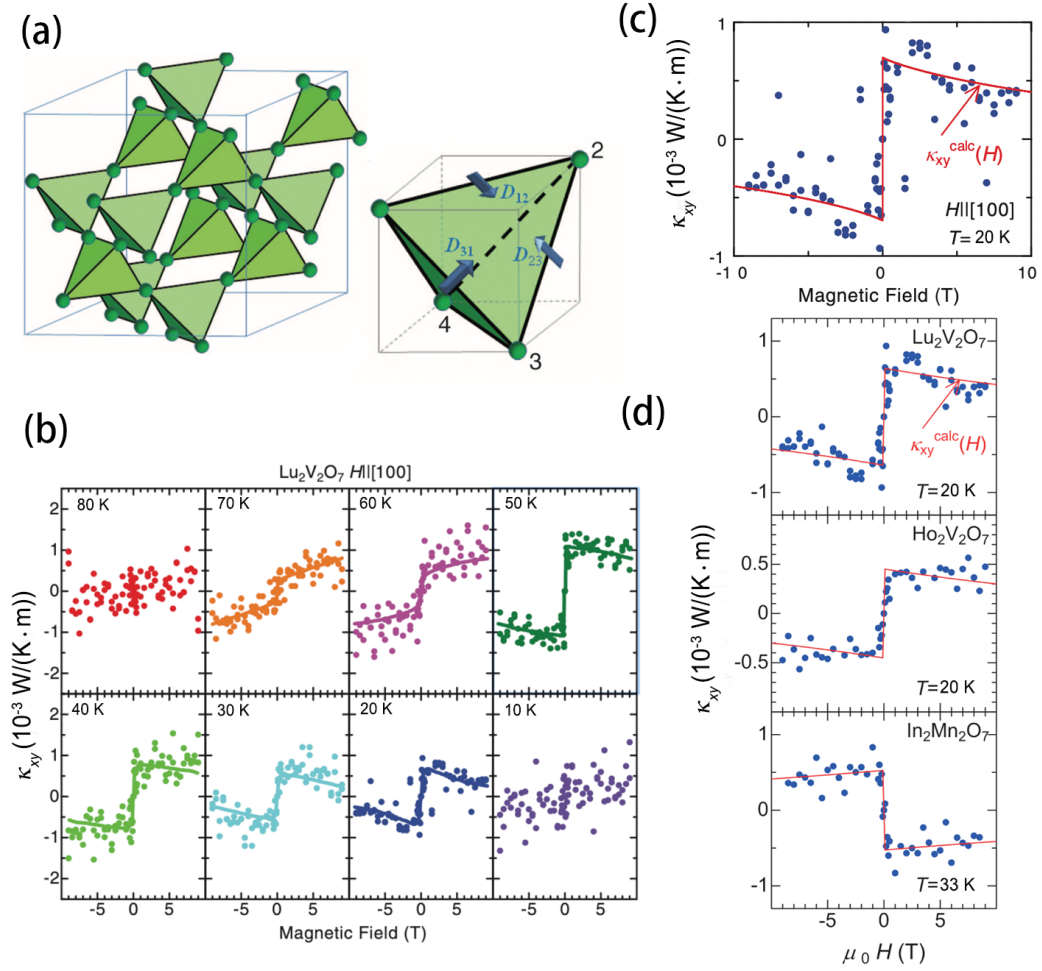


Fig. 2. (a) The crystal structure of $\text{Lu}_2\text{V}_2\text{O}_7$ and the direction of the DM vector \mathbf{D}_{ij} on each bond of a tetrahedron^[28]. (b) Magnetic field variation of the thermal Hall conductivity of $\text{Lu}_2\text{V}_2\text{O}_7$ at various temperatures^[28]. Solid lines are guides to the eye. (c) Magnetic field variation of the thermal Hall conductivity at 20 K for $H \parallel [100]$ ^[28]. The red solid line indicates the magnetic field dependence given by the theory (Eq. 11). (d) Magnetic field variation of thermal Hall conductivity for $\text{Lu}_2\text{V}_2\text{O}_7$, $\text{Ho}_2\text{V}_2\text{O}_7$, $\text{In}_2\text{Mn}_2\text{O}_7$ ^[33]. Red solid lines are given by the theory (Eq. 12).

Nijs (TKNN)-type formula for non-interacting bosons and it is corrected to

$$\begin{aligned} \kappa_{\alpha\beta} &\approx 2T \int_{\text{BZ}} \frac{d^3k}{(2\pi)^3} c_2[\rho_1(\mathbf{k})] \text{Im} \left(\frac{\partial \psi_1(\mathbf{k})}{\partial k_\alpha} \middle| \frac{\partial \psi_1(\mathbf{k})}{\partial k_\beta} \right) \\ &= \Phi_{\alpha\beta} \frac{4k_B^2 T}{3\pi^2 \hbar a} \left(\frac{k_B T}{2JS} \right)^{5/2} \int_0^\infty c_2 \left(\frac{t^{3/2}}{e^{t + \frac{g\mu_B H}{k_B T}} - 1} \right) dt \\ c_2(\rho) &= (1 + \rho) \left(\lg \frac{1 + \rho}{\rho} \right)^2 - (\lg \rho)^2 - 2\text{Li}_2(-\rho), \end{aligned} \quad (12)$$

considering the rotational motion of magnons^[33,47]. The corrected theoretical outcome is compared with the experimental data in Fig. 2(d). In other similar materials, $\text{Ho}_2\text{V}_2\text{O}_7$ and $\text{In}_2\text{Mn}_2\text{O}_7$, κ_{xy} are calculated and compared with experiments^[33]. The high consistency

between experimental and theoretical results strongly supports the magnon scenario of THE in $\text{Lu}_2\text{V}_2\text{O}_7$. The successful theoretical explanation connects the DMI and the Berry curvature, pointing out a new way to generate nontrivial Berry curvature, and all of these can be verified experimentally by THE by measuring κ_{xy} .

2. $\text{Cu}(1,3\text{-bdc})$

$\text{Cu}(1,3\text{-bdc})$ is another material with nonzero DM vectors. In this example, we can see clearly how the magnetic field induces nontrivial Berry curvatures and consequently a finite THE. As illustrated in Fig. 3(a), $\text{Cu}(1,3\text{-bdc})$ is a kagome ferromagnet with weak anti-

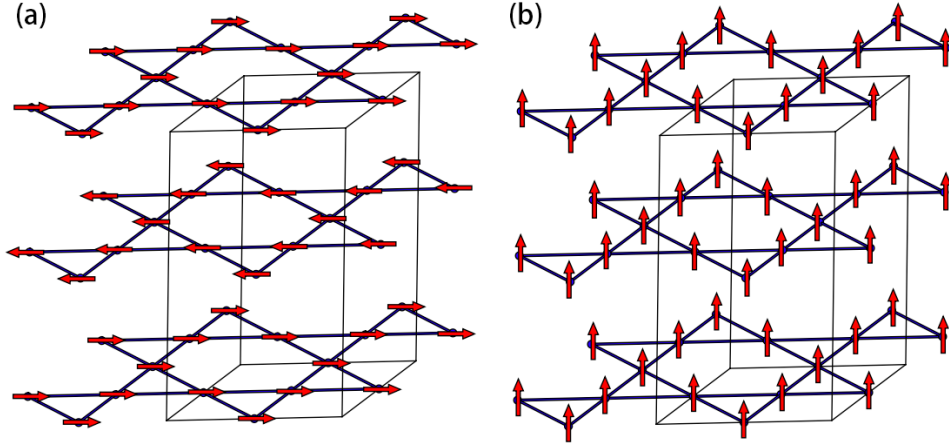


Fig. 3. Magnetic structure of Cu(1,3-bdc) without (a) and with (b) a perpendicular magnetic field^[34].

ferromagnetic interlayer interaction and strong in-plane ferromagnetic interaction^[34]. The moments lie in the kagome plane but it can be fully polarized easily along the c -axis with a small magnetic field ($\mu_0 H \approx 0.05$ T), as shown schematically in Fig. 3(b). The DM vectors point along the c -axis and it is convenient to make spins parallel to \mathbf{D} .

In Ref.^[46], it is shown that the longitudinal thermal conductivity κ_{xx} of Cu(1,3-bdc) grows abruptly around $T = T_c = 1.8$ K (Fig. 4(a)) and becomes field dependent, implying spins contribute to the thermal conductivity below T_c . By subtracting the phonon background κ_{ph} measured in the high field from κ_{xx} , one can obtain the part contributed by spins as defined by $\kappa_s \equiv \kappa_{xx} - \kappa_{ph}$. The thermal Hall conductivity is also measured. When a magnetic field parallel to c -axis is applied, the thermal Hall conductivity grows from zero and it is an odd function of H_c . It is interesting that both κ_s and the thermal Hall conductivity κ_{xy} have the activated form [Fig. 4(b)], indicating both come from the same carriers—magnons^[46].

$$\kappa_{xy(s)} \rightarrow T \exp[-\beta \Delta] \quad (\Delta = g\mu_B H). \quad (13)$$

Chisnell et al. later on showed inelastic neutron scattering data on the magnon bands which are helpful in understanding the thermal and thermal Hall conductivity results^[34]. The experimental data in zero and finite fields are shown in Fig. 4(c1-c3). It is clear to see that an external field perpendicular to the kagome plane opens two gaps separating the three magnon

bands (Fig. 4(c2) and especially Fig. 4(c3)). They also calculated the spin-wave dispersion using the Holstein-Primakoff transformation. The calculated spectra are shown in Fig. 4(c4). Compared the calculations with the experimental data, it is found that gaps opened by the perpendicular magnetic field lead to nontrivial magnon bands with Chern numbers -1, 0 and 1 for the lowest, middle, and highest energy bands, respectively. In addition, they compared the calculated dynamic structure factor for the spin waves $\mathbf{S}(\mathbf{Q}, \omega)$ with neutron scattering data. In order to avoid nonmagnetic background, they examined the differences in densities at two different applied fields, as shown in (Fig. 4(d)). It is pleasing to see that the theory and the experiment are in high agreement.

In this example, the magnetic field plays such a role that it no longer acts directly on the quasiparticles, providing the Lorentz force, but rather “activates” the DMI by turning the direction of spins to that of the DM vectors. It is the DMI, as a perturbation to the next-nearest Hamiltonian, that opens the gaps between three magnon bands, yielding topologically nontrivial bands. And therefore, the nontrivial Berry curvature or the possible chiral edge modes can be responsible for the magnon THE^[34].

3. Perovskite Oxides

The geometry and symmetry of lattice are able to have a great impact on the Berry curvature. In our

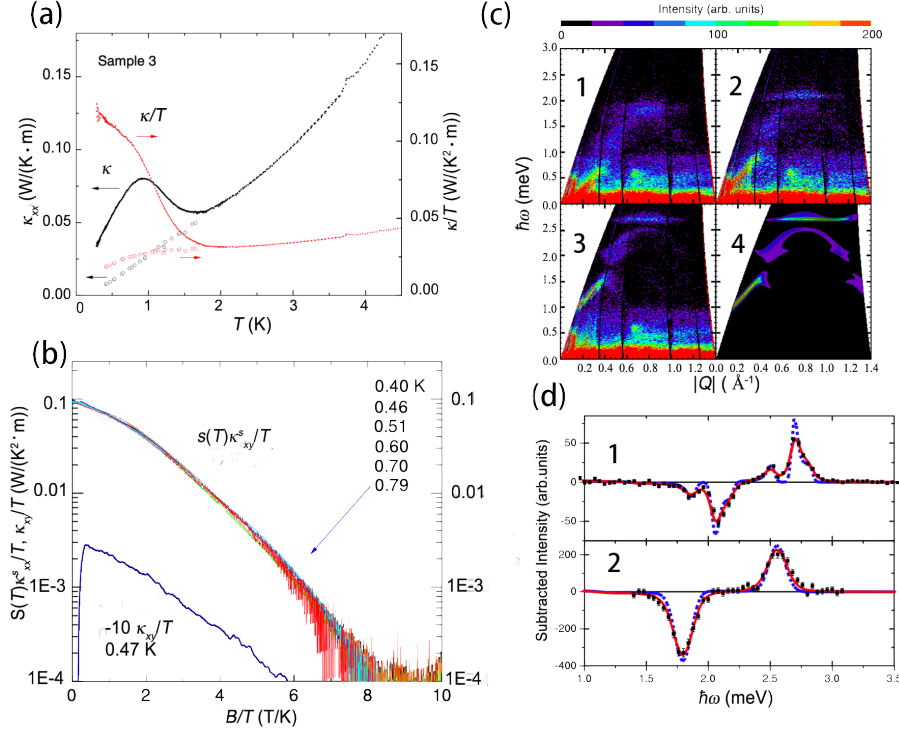


Fig. 4. (a) κ (black symbols), κ/T (red symbols) and their values in large magnetic fields (open symbols) which are identified to be the phonon background^[46]. (b) The slope in a large field gives a Zeeman gap with $g = 1.6$. The Hall curve κ_{xy}/T has a similar slope in a large fields^[46]. (c) (1-3) Inelastic neutron scattering spectra at $T = 1$ K, with field (1 zero field, 2 $\mu_0 H = 2$ T and 3 $\mu_0 H = 7$ T) perpendicular^[34]. (d) Quantitative comparison with the intensities calculated from the deduced spin Hamiltonian. Data points in (1) correspond to the difference in intensities at $\mu_0 H = 7$ T and $\mu_0 H = 2$ T with the field perpendicular to the plane, and those in (2) correspond to the difference in intensities at $\mu_0 H = 7$ T and $\mu_0 H = 0$ T with the field parallel to the plane^[34].

discussions above, the symmetry restrains the direction of DM vectors through Moriya's Law and thus affects the thermal Hall conductivity. In this example, the influence of geometry and symmetry on the thermal Hall conductivity can be further clarified through a comparison between two different perovskite oxides with similar lattice structures but with actually different lattice geometries. The first material is BiMnO₃, the structure of which is distorted due to Bi 6s² lone pair^[48], which lowers the symmetry of the whole crystal and allows a nonzero-DM vector. Another important factor is its very special orbital ordering^[33]. It enlarges the unit cell of BiMnO₃, in which there are 16 Mn atoms. The second material is YTiO₃, which has the GdFeO₃-type orthorhombic crystal structure^[33]. Usually there is antiferromagnetic interaction between the nearest-neighboring magnetic moments of transition metals in perovskite Mott insulators^[33], while the two materials above both stabilize the ferromagnetic

order by orbital ordering^[33,49].

It is of great importance that in YTiO₃, the magnon Hamiltonian containing DMI is invariant under the following transformation (Eq. 14), from which the Berry curvature can be proved to be zero when the magnetic field is applied along x or z -axis.

$$(\Sigma^x H(k) \Sigma^x)^* = H(k), \quad \Sigma^x = \begin{pmatrix} 0 & 0 & 1 & 0 \\ 0 & 0 & 0 & 1 \\ 1 & 0 & 0 & 0 \\ 0 & 1 & 0 & 0 \end{pmatrix}. \quad (14)$$

Eq. 12 shows that if the Berry curvature vanishes, the thermal Hall conductivity must be zero. And it is consistent with the experimental data, where BiMnO₃ has nonzero thermal Hall conductivity while YTiO₃ does not, as shown in Fig. 5.

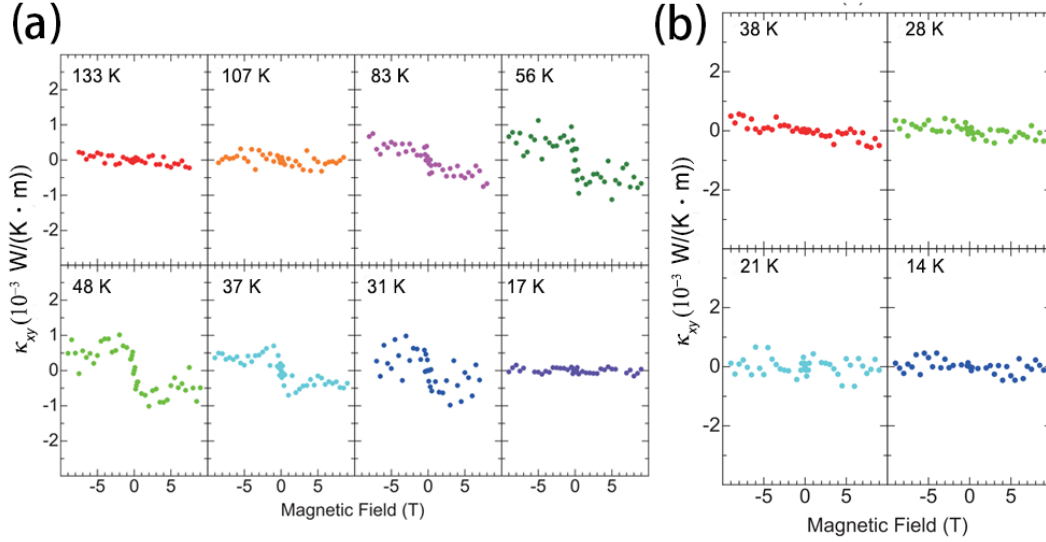


Fig. 5. Magnetic field variation of the thermal Hall conductivity at different temperatures of BiMnO₃ (a) and YTiO₃ (b)^[33].

B. Phonon Hall Effect

Since the phonon Hall effect was first observed in Tb₃Ga₅O₁₂^[50], it has not attracted much attention. One of the reasons is that phonon is charge neutral thus it cannot be directly affected by magnetic fields. Therefore, the phonon Hall effect has been considered very weak. However, it is found that in SrTiO₃, a paraelectric and nonmagnetic insulator (which means phonons are the only possible carriers), the κ_{xy} can reach up to 80 mW/(K·m)^[51], far exceeding the expectation. The discoveries and explanation of the enhanced phonon Hall effect have broadened the horizon of THE and shed new light on the materials with giant THE.

The experimental results of thermal and thermal Hall conductivity on SrTiO₃ are shown in Fig. 6(a) and (b). It is found that κ_{xy} varies with samples but κ_{xx} and κ_{xy} always peak at the same temperature (implying the same dominant heat carriers) and κ_{xy} decreases much faster than κ_{xx} at both sides of the peak. In addition, it seems that κ_{xy} can even be changed after warming up above the antiferrodistortive transition temperature and cooling back for the same sample. In order to clarify the origin of the large THE, the heat transport in KTaO₃ is also investigated. Compared with SrTiO₃, KTaO₃ does not undergo an antiferrodistortive transition and its low-temperature electric permittivity is five times smaller. As is shown in Fig. 6(d), the thermal

Hall conductivity of KTaO₃ is much smaller than that of SrTiO₃. Here comes a question that whether it is the antiferrodistortive transition (the domains) or the electric permittivity that accounts for the large phonon Hall effect.

Later, Chen et al. elucidated that it was the domain that resulted in the enhanced THE^[40]. The team first considered the intrinsic thermal Hall conductivity which, similar to the magnon Hall effect, originated from the nonzero Berry curvature and was totally determined by the Berry curvature and dispersions of the phonon bands^[20]. Though amplified by the electric permittivity $\chi \approx 2 \times 10^4$, the intrinsic thermal Hall conductivity κ_{xy}^{in} as calculated by Eq. 15 is still four orders of magnitude smaller than the observed value.

$$\frac{\kappa_H^{\text{in}}}{\kappa_L} \sim \frac{\chi \epsilon_0 F B T}{K c \hbar} \frac{v \hbar}{T \ell}, \quad (15)$$

where κ_H is the intrinsic thermal Hall conductivity, κ_L the thermal conductivity, χ the electric permittivity, ϵ_0 the permittivity of vacuum, F the flexoelectric coupling coefficient, B the magnetic field, T the temperature, K the elastic moduli, c the speed of light, \hbar the reduced Planck constant, v the sound velocity and ℓ is the phonon mean free path.

Since the intrinsic factors alone cannot explain the huge THE, the team soon resorts to extrinsic factors. They assume there exist dilute defects (in STO it could

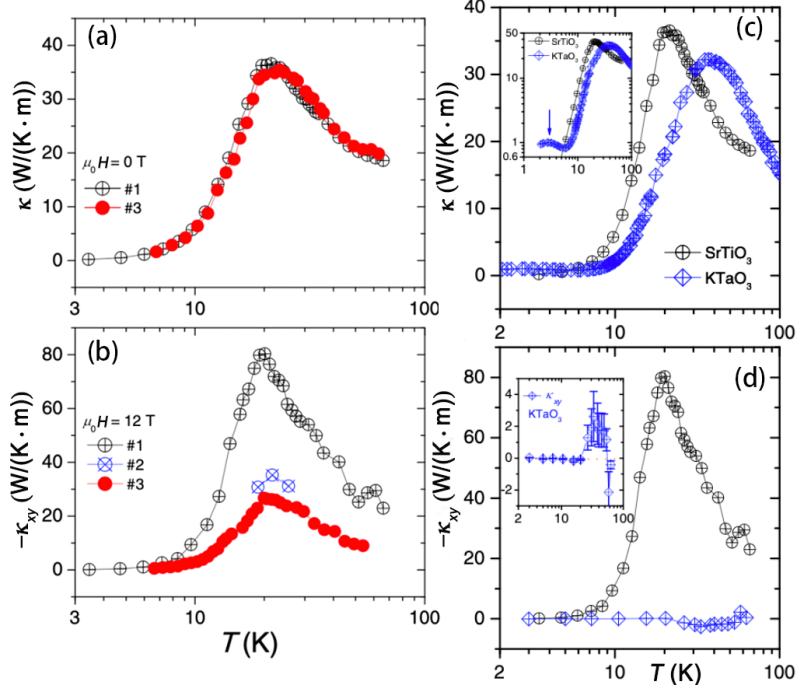


Fig. 6. κ_{xx} and κ_{xy} as a function of temperature for SrTiO₃ ((a), (b)) and KTaO₃ ((c), (d))^[51].

be the domains coming from the AFD transition) that scattered phonons strongly and Eq. 15 can be modified to Eq. 16,

$$\frac{\kappa_H^{\text{ex}}}{\kappa_L} \sim 5A \frac{\chi \epsilon_0 F B T}{K c \hbar}, \quad (16)$$

where κ_H^{ex} is the extrinsic thermal Hall conductivity and A a dimensionless strength to describe how much the Berry curvature would affect the skew scattering.

After taking into account the extrinsic factors, the thermal Hall conductivity that originated from the non-trivial Berry curvature is much enhanced. The resulting κ_{xy} has a similar magnitude as the experimental data. Furthermore, the new formula also predicts $\kappa_{xy} \propto T^4$ since $\kappa_{xx} \propto T^3$, which explains the observation that κ_{xy} decreases faster than κ_{xx} on the low-temperature side. Additionally, it can also explain the absence of κ_{xy} in KTaO₃, as there is no antiferrodistortive transition in KTaO₃, and thus no antiferrodistortive domains to scatter phonons.

C. Materials with Controversial Origins of THE

As this is still the early stage on the research of THE, the origin of thermal Hall conductivity in vari-

ous materials is still mysterious, or under debate. In the following, we discuss THE in quantum-spin-liquid candidate α -RuCl₃, multiferroic Fe_{1-x}Zn_xMo₃O₈, and cuprate superconductors La_{2-x}Sr_xCuO₄ as examples.

1. α -RuCl₃

Quantum spin liquid is a special state where there exists a high degree of entanglement and fractional excitations^[52,53]. Excitations carrying fractional quantum numbers manifest novel topological properties, and the predicted non-Abelian quasiparticles can have applications in quantum computation^[54–56]. Furthermore, studying quantum spin liquids may shed light on the mechanism of the high-temperature superconductivity^[57]. To explore the exotic properties in quantum spin liquids, people have been keeping searching for candidate materials in frustrated magnets^[52], which mainly include materials with triangular lattice^[58–62], kagome lattice^[53,63–67], and honeycomb lattice^[68–70]. Among them, α -RuCl₃ has been studied extensively recently^[71,72].

The material α -RuCl₃ is quasi-two-dimensional with Ru atoms forming a honeycomb lattice and each magnetic atom shows $J_{\text{eff}} = 1/2$ because of spin-

orbit coupling and crystal field^[71,73,74]. The magnetic behavior can be described by a minimal “K- Γ ” model^[75], in which the Γ and possibly other smaller longer-range terms stabilize a zigzag antiferromagnetic state below $T_N \approx 7.5$ K without magnetic field^[76]. The in-plane lattice structure is shown in Fig. 7(a). The b -axis (the armchair direction), possesses a two-fold symmetry while the a -axis does not. Fig. 7(b) and (c) show different stacking forms, and particularly, dashed lines in Fig. 7(b) and (c) indicate a perfect and faulty stacking, respectively. The latter is common in quasi-two-dimensional materials. The stacking fault will suppress the transition signal of the as-grown single crystal at T_{N1} and induce another transition at a higher temperature T_{N2} , making the curve closer to that of the powder, as shown in Fig. 7(d)-(f).

In this material, there have been three different perspectives on the type of heat carriers by now. The first one is the Majorana fermions, whose antiparticles are themselves. The Majorana fermions are predicted to occur in the Kitaev quantum spin liquids and they are proposed to exist in α -RuCl₃^[78]. Since Majorana fermions are charge-neutral particles, they can only conduct heat, with the thermal Hall conductivity having the special form:

$$\kappa_{xy}^{2D}/T = c(\pi/6) (k_B^2/\hbar), \quad (17)$$

where $\kappa_{xy}^{2D} \equiv \kappa_{xy} \cdot d$ (d is the interlayer distance), k_B , \hbar , and $c = 1/2$ are the Boltzmann constant, reduced Planck constant, and the central charge in α -RuCl₃^[81,82], respectively.

It was first reported that, applying a perpendicular magnetic field $\mu_0 H_z = 12$ T, the κ_{xy} changed sign from negative to positive when the temperature rose above the T_N , indicating different origins of κ_{xy} before and after the transition^[83]. The field-dependent κ_{xy} also implies spin excitations contribute significantly in the system. Then, the plateau of κ_{xy}/T (Eq. 17) was observed with the magnetic field tilted in the a - c plane, and the heat flow \mathbf{q} parallel to the a -axis^[81], as shown in Fig. 8. Although the plateau can only exist below 5.5 K, it strongly indicates the existence of the Majorana fermions. The phase diagram is given in Fig. 9 accordingly. Bruin et al.^[84] then conducted a comprehensive study of the thermal Hall conductivity

and demonstrated that the approximate half-integer quantization existed in a much-extended region of the phase diagram, which proved the robustness of the quantum plateau.

Later on, Yokoi et al. present another piece of evidence trying to strengthen the Majorana point^[27]. First, they compare the results with fields applied along a and b -axes at $T = 4.8$ K. With $\mathbf{q} \parallel a$, the plateau occurs only when the field is applied along the a -axis with field strength exceeding the critical field that fully suppresses the magnetic order, as shown in Fig. 10(a). The result is explained as follows: the absence of κ_{xy} for $H \parallel b$ was attributed to the two-fold symmetry of the b -axis,

$$\kappa = U^T \kappa U \quad (18)$$

where U is the rotation matrix $\begin{pmatrix} 1 & \\ & -1 \end{pmatrix}$. The plateau which preserves without a perpendicular field implies that the thermal Hall conductivity arises from a topologically non-trivial Chern insulator of Majorana fermions.

Second, they compare the results with fields applied along a and $-a$ -axes, but with a finite out-of-plane field component, as shown in Fig. 10(b). The result is indeed interesting. After the critical field, κ_{xy} in different conditions are both quantized but exhibit different signs, while below the critical field, κ_{xy} has the same sign and is nearly the same in quantity. The former is precisely explained by the Kitaev theory, which predicts the sign changes with different directions of the magnetic field, as shown in Fig. 10(c). The latter is assumed to be induced by the magnon Hall effect, which is closely related to the out-of-plane magnetic field.

The results and explanations above are to some extent plausible and convincing, but the experimental results, especially the half-quantized plateau of κ_{xy} , are still not observed by many independent groups. That is the reason why this point of view is highly controversial.

The second perspective is that the thermal Hall effect originates from the phonon Hall effect. The main reason is that according to experimental results, the curves of κ_{xx} and κ_{xy} are similar and can be both understood by a phonon scenario. Hentrich et al. have

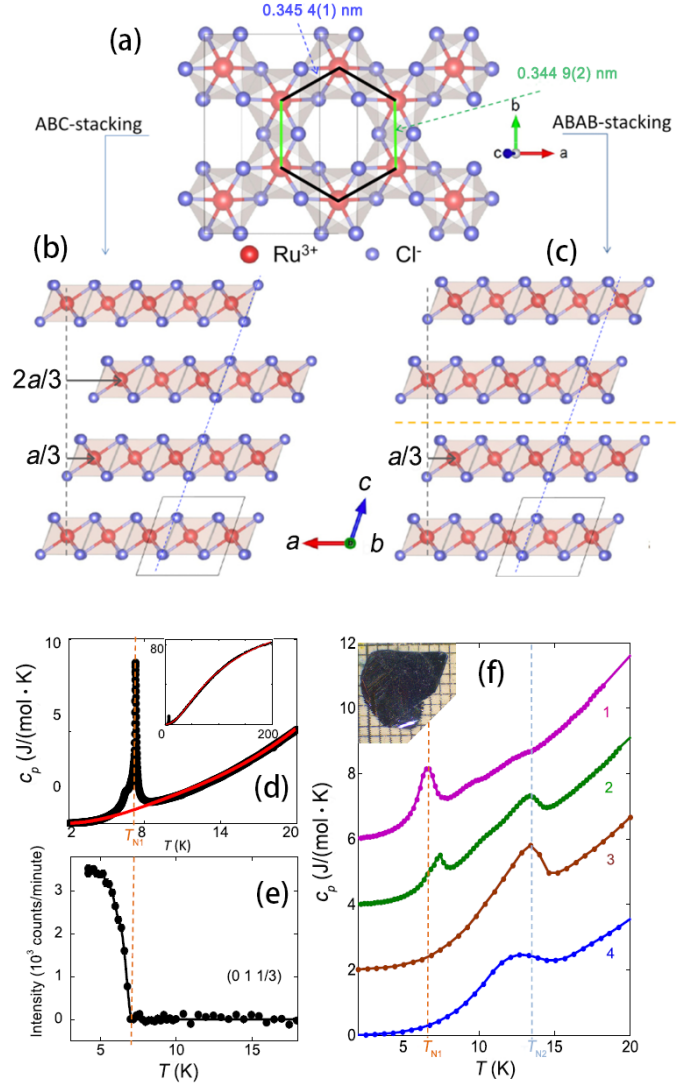
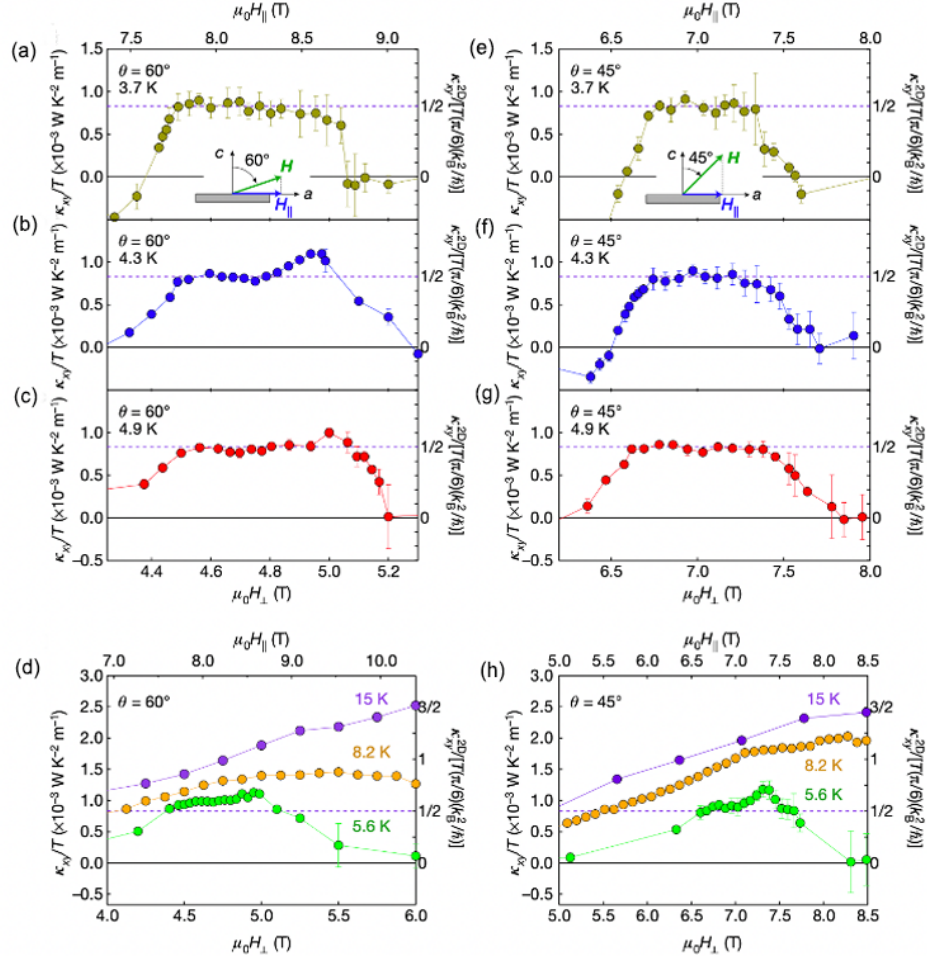
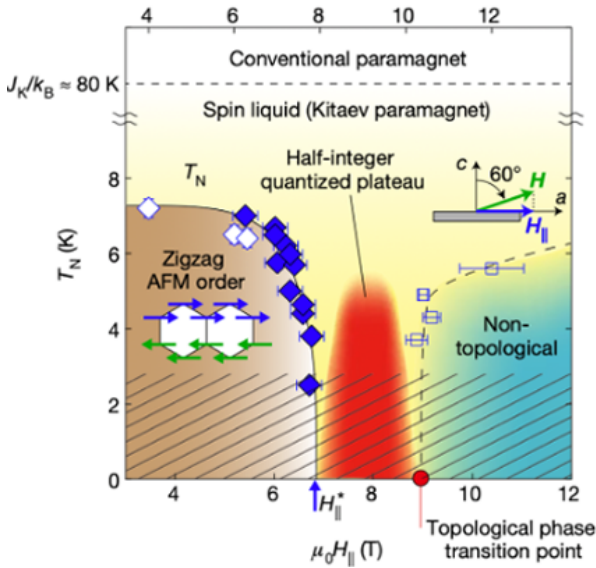


Fig. 7. (a) The in-plane structure of layered compound α - RuCl_3 viewed perpendicular to the layers along the c^* -axis. (b) ABC stacking: the out-of-plane structure viewed along the b -axis. (c) ABAB stacking: viewed in the same orientation as that in (b). (d) The heat capacity of an as-grown single crystal of α - RuCl_3 from 2–20 K shows the low-temperature region exhibiting one sharp Néel transition at $T_N = 7$ K. (e) The thermal evolution of the intensity of the magnetic peak (0, 1, 1/3). (f) The heat capacity data on the same single crystal when subject to artificial deformation (1–3). (4) is from the powder sample^[77].

found unusual behavior of the thermal transport in α - RuCl_3 ^[85]. They apply an in-plane magnetic field and measure κ_{xx} in the a - b plane (κ_{ab}) and along c -axis (κ_c). From Fig. 11(a), it seems that there are two regimes according to the B and T dependences of the thermal conductivity, divided by $B_c \approx 7.5$ T. In regime I, κ slightly decreases as the field increases, which is especially evident for $T < T_N$, indicating the suppression of the long-range magnetic order. While in regime II, κ apparently increases with the field.

Fig. 11(a2) shows that in regime II, there is always a low-temperature dip, explained by a gap originating from the magnetic excitations. (A “dip” refers to a tendency where κ goes down first and then increases, which is not so obvious in Fig. 11(a2) for the x -axis being stretched.) The regimes are distinctive, as shown in Fig. 11(c). For the zero-field curve, κ decreases as the temperature increases up to T_N , which implies the suppression of the long-range magnetic order. Above T_N , κ increases rapidly. The phononic heat conduc-


 Fig. 8. The quantum plateau of thermal Hall conductivity observed in α -RuCl₃^[27].

 Fig. 9. The phase diagram of α -RuCl₃ obtained according to the results in Fig. 8^[81].

tivity can be estimated as $\kappa_{\text{ph}} \approx c_V v l$, where the velocity v and the mean free path l are nearly temperature independent and the specific heat c_V grows with temperature, and therefore κ increases with temperature. For higher temperatures, the mean free path is reduced by phonon Umklapp processes, leading to a broad peak followed by a fast decline. For the $B = 16$ T curve, one significant signature is that κ is much larger than that in the zero fields, and another typical feature is the low-temperature dip mentioned earlier. The two features are both explained by the phonon scattering of the magnetic excitations. In regime I, magnetic excitations are low-energy and nearly gapless, and thus phonons can be scattered strongly. In regime II, magnetic energy is lifted and a gap opens, which is marked with $\hbar\omega_0$. Therefore, the dip appears naturally when the energy of dominant excited phonons is around $\hbar\omega_0$, where phonons are scattered strongly by magnetic

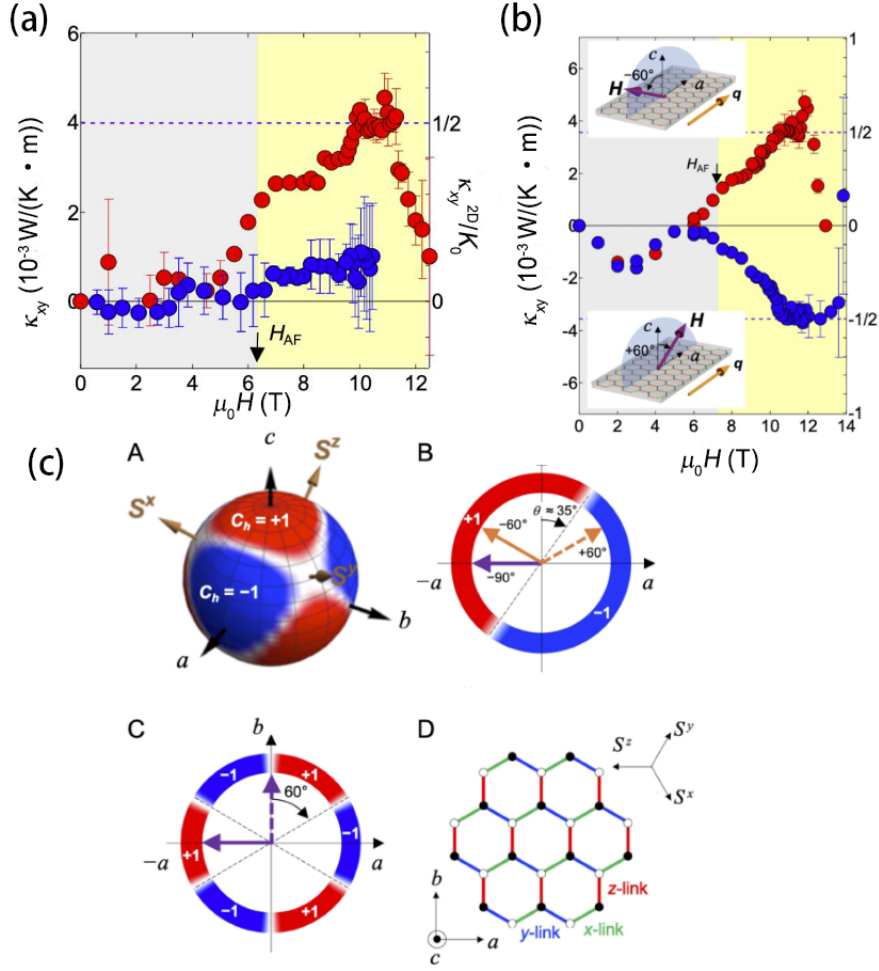


Fig. 10. (a) Thermal Hall conductivity κ_{xy} in the antiferromagnetic (gray shaded area) and spin liquid (yellow area) states for $\mathbf{H} \parallel -a$ -axis (red circles) and $\mathbf{H} \parallel b$ -axis (blue circles) at 4.8 K. (b) Field dependence of κ_{xy} at 4.3 K in tilted field of $\theta = -60^\circ$ (red circles) and 60° (blue circles) away from the c -axis in the a - c plane. (c) Theoretical results for the field-angular variation of the sign (C_h) of κ_{xy} [27].

excitations. In this way, $\hbar\omega_0 \approx k_B T$ can be estimated accordingly, which is shown in Fig. 11(d). Furthermore, a phenomenological model considering magnetic scattering is used to fit the experimental results, which turns out to show high consistency with the experimental data, as shown in Fig. 11(b). Additionally, the curves of κ_{ab} are quite similar to those of κ_c , indicating the predominant heat carriers are phonons since spin-dominated effects will have more distinct differences for a two-dimensional material.

Lefrançois et al. provided another evidence for phonon Hall effect in α - RuCl_3 [86]. κ_{xx} and κ_{xy} of five crystals from two different sources are measured, with heat current $\mathbf{q} \parallel a$. As shown in Fig. 12, the curves

of κ_{xx} and κ_{xy} from five different samples are indeed similar qualitatively and the quantities are very sample dependent. The qualitative behavior of κ_{xx} without a magnetic field is consistent with those in Fig. 11(c). These all indicate a phononic picture and the sample dependence is attributed to different levels of disorder.

Moreover, they argued that the magnitude of the thermal Hall angle $|\kappa_{xy}/\kappa_{xx}| \approx 1 \times 10^{-3}$ was typical for the phonon thermal Hall effect. In this spirit, κ_{xy} larger or smaller than the half-quantized value could be well explained by the different abilities of phonons to conduct heat in different materials. In addition, they compare thermal transport with and without in-plane magnetic field, as shown in Fig. 12(c) and (d) and it

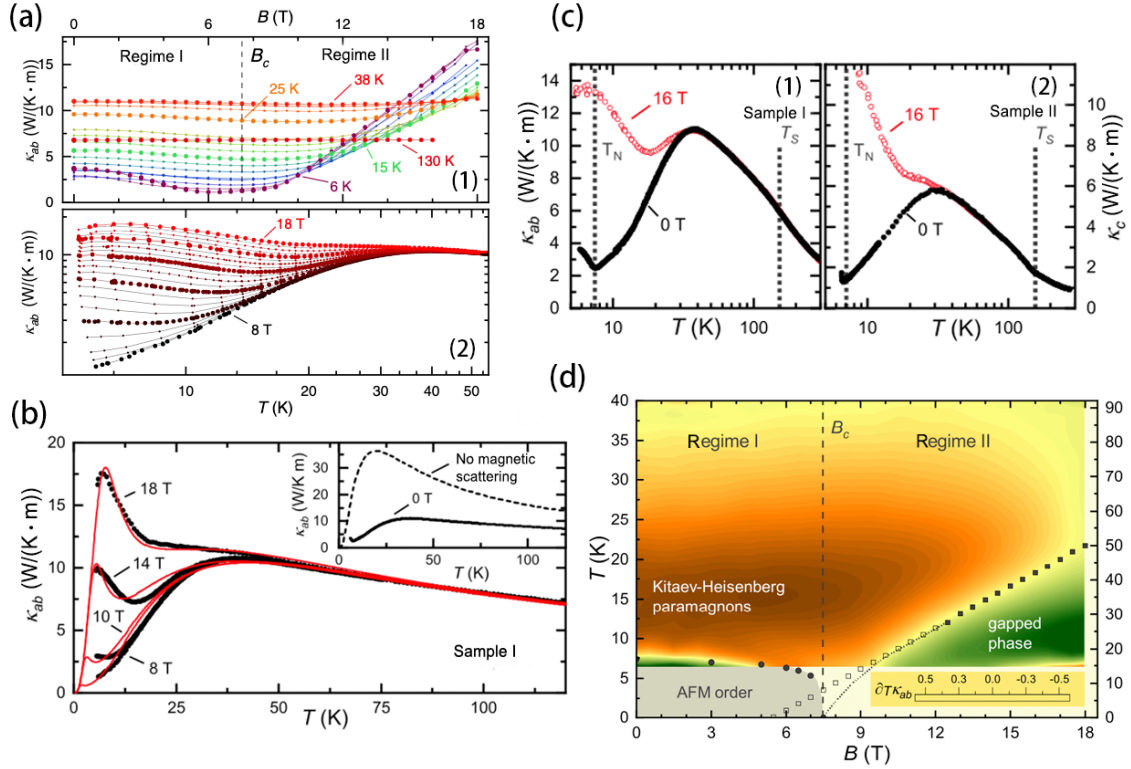


Fig. 11. (a) Magnetic field and temperature dependences of the heat conductivity of α -RuCl₃ (sample I). (b) κ_{ab} data of sample I (solid circles) and fits (solid lines) to the Callaway model for selected magnetic fields. (c) Temperature dependence of the heat conductivity of α -RuCl₃ at $\mu_0 H = 0$ and 16 T for κ_{ab} (sample I in (1)) and κ_c (sample II in (2)). (d) False-color representation of the temperature derivative $\partial\kappa_{ab}/\partial T$ (sample I) together with the gap energy $\hbar\omega_0/k_B$ (solid squares) extracted from the phononic fits^[85].

turns out that κ_{xx}/T and κ_{xy}/T no longer increased at low temperatures, which is plausible for phonons since the in-plane magnetic field could destroy the long-range order. It is also clear to see that κ_{xy} is much smaller than the quantized value κ_{HQ} . Therefore, from this perspective of view, phonons play an important role in the thermal transport in α -RuCl₃ and the plateau observed before^[27,28] could only exist only if phonons' contributions are approximately zero which is unlikely to occur.

The third and last point of view is that there might be a Fermi surface in α -RuCl₃ since a “de Haas–Van Alphen-like” effect is observed^[44], and thus another kind of fermion rather than the Majorana fermion may come into play. In Ref.^[44], they first apply a magnetic field H and thermal flow \mathbf{q} both parallel to the a -axis and find that κ_{xx} oscillates with a field below 4.5 K, as shown in Fig. 13(a). This is more clearly shown in Fig. 13(b), the oscillation starts from about $\mu_0 H = 4$ T

and after $\mu_0 H$ exceeds 11 T, κ_{xx} suddenly saturates. It seems that the state between $4 \text{ T} < \mu_0 H < 7 \text{ T}$ is a mixture of the zigzag antiferromagnetic state and the possible quantum spin liquid state, while the quantum spin liquid and paramagnetic states have a distinct border at $\mu_0 H = 11$ T. Fig. 13(c) shows that κ_{xx} , regardless of the direction of the magnetic field, is periodic with the in-plane component of the field $1/\mu_0 H_a$. The oscillation is also reproducible across samples, which enhances the reliability and implies it is intrinsic in the quantum spin liquid state. Additionally, the half-quantized plateau is not observed in Fig. 13(d).

A brief summary of the thermal transport results on α -RuCl₃ is presented here. The evidence of Majorana quasiparticles is the half-quantized plateau and the sign changes of κ_{xy} explained successfully by the Kieav theory, but the phenomenon is difficult to be reproduced by other independent groups. The evidence of the Fermi surface is the oscillation of κ_{xx} with

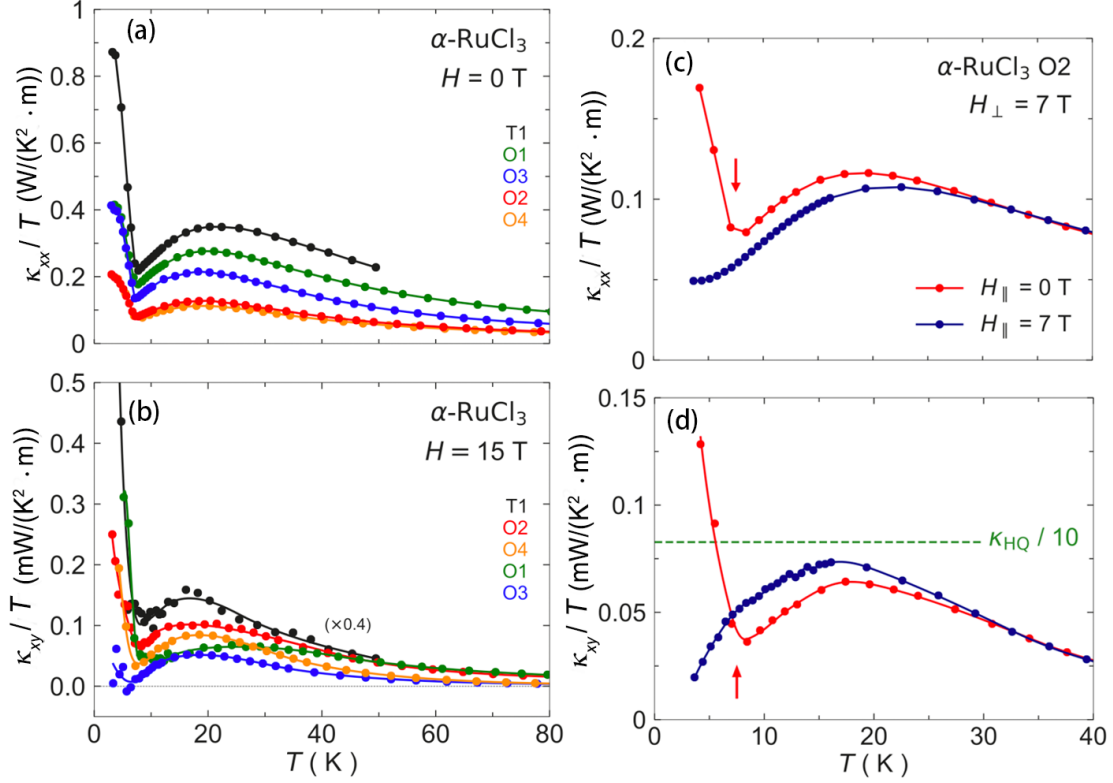


Fig. 12. (a) Thermal conductivity of α -RuCl₃ in zero magnetic field for five different samples. (b) Thermal Hall conductivity of the same five samples, measured in a magnetic field of $\mu_0 H = 15$ T applied normal to the honeycomb layers. (c) Thermal conductivity κ_{xx} of sample O2. (d) Same as in (c) but for κ_{xy} . The horizontal dashed line marks the quantized value (κ_{HQ}) expected for Majorana edge modes, divided by 10. Arrows mark the T_N .^[86]

$1/\mu_0 H_a$. The common feature in these results is that the phenomena are observed in a narrow temperature range. However, the evidence for phonons is gained by analyzing the similar behavior of κ_{xx} and κ_{xy} in a large temperature range.

2. Multiferroics $(\text{Fe}_{1-x}\text{Zn}_x)_2\text{Mo}_3\text{O}_8$

Multiferroics, where elementary excitations are strongly influenced by lattice-spin coupling, manifest novel thermal transport properties. Recently, the giant THE in insulating polar magnets $(\text{Fe}_{1-x}\text{Zn}_x)_2\text{Mo}_3\text{O}_8$ is observed^[87]. By now, the giant κ_{xy} in this material has been assumed to be dominated by phonons, but extremely sensitive to the magnetic structure. The microscopic mechanism is still under investigations.

The crystal structure and magnetic phase diagram of $(\text{Fe}_{1-x}\text{Zn}_x)_2\text{Mo}_3\text{O}_8$ are shown in Fig. 14. It is clear to see in Fig. 14(b) that each magnetic layer (the two Fe atoms with tetrahedral and octahedral oxygen

coordinations) forms a honeycomb lattice, and the DM vectors (Eq. 8) lie in the a - b plane. Therefore, as is the case in the following discussion, when applying a perpendicular field, the conventional magnon Hall effect vanishes.

The specific heat shown in Fig. 15(a) is proportional to T^3 below 32 K both in zero and high magnetic fields, indicating phonon-like excitations at low temperatures. High similarity in quantities also implies that the magnetic field will not affect the population of the quasiparticles. The thermal conductivity κ_{xx} shows abnormal behavior (Fig. 15(b)). The peak around 15 K is probably due to the decrease of the mean free path and the increase of the population. In this case, the suppression of κ_{xx} before $T_N \approx 60$ K in the high field can only be explained by the suppression of the mean free path, which is contradictory to the phonon scenario. This contradiction is assumed to be caused by the strong lattice-spin interaction in multiferroics since the population of spin excitations

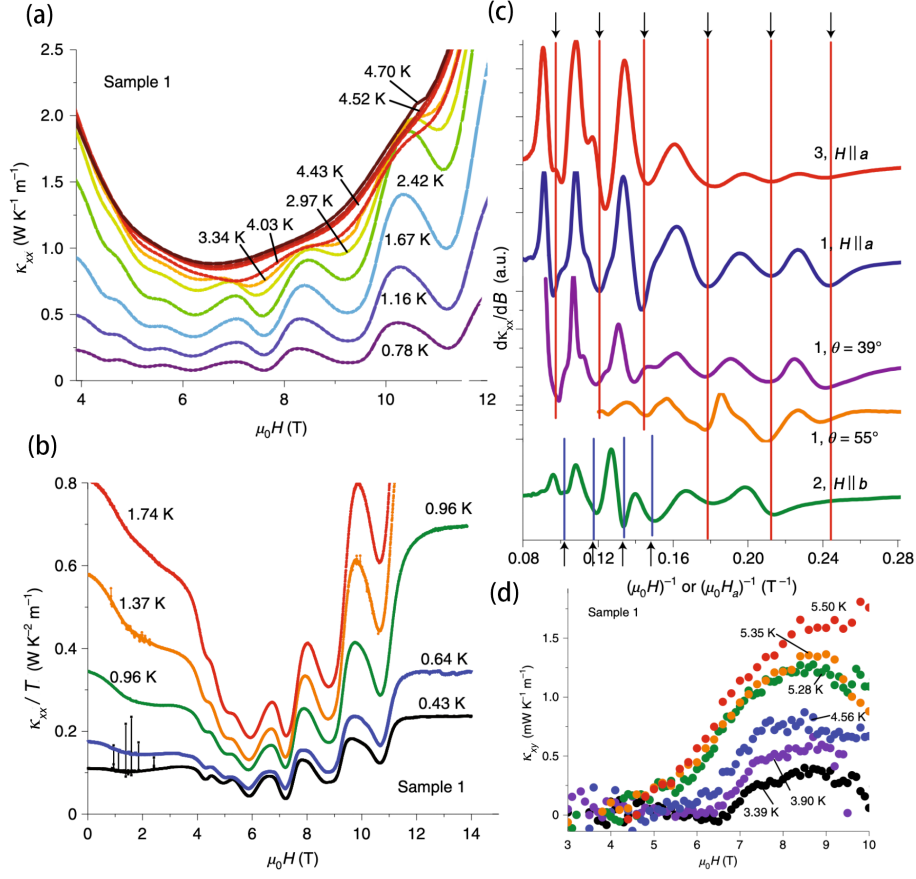


Fig. 13. (a) The emergence of oscillations in $\kappa_{xx}(\mathbf{H} \parallel \mathbf{a})$ at low temperatures. (b) The oscillations over the full field range at selected temperatures. (c) Curves of the derivative $d\kappa_{xx}/dB$ versus $1/H$ (or $1/H_a$) in arbitrary units (a. u.) for Samples 1, 2 and 3 ($H_a = H \cos \theta$). (d) Magnetic field variation of the thermal Hall conductivity at different temperatures of $\alpha\text{-RuCl}_3$ [44].

decreases under a magnetic field. The thermal Hall conductivity κ_{xy} , as shown in Fig. 15(c), also manifests different behaviors below and above the transition temperature $T_N \approx 50$ K. Below T_N , κ_{xy} reaches its maximum quickly and decreases slowly with field, while above T_N , κ_{xy} increases slowly with the field, indicating different mechanisms to generate κ_{xy} in different temperature regions. In addition, κ_{xy} is one-magnitude larger than the value of $\kappa_{xy} \sim 1 \text{ mW/K m}$ in common systems, while the thermal Hall angle is still small, with $|\kappa_{xy}/\kappa_{xx}| \approx 10^{-3}$.

3. Cuprate High-Temperature Superconductors

High-temperature superconductivity in copper oxides (“cuprates”) still fascinates physicists for the novel quantum phenomena in these materials. It

is a common belief^[88] that the basic difficulties are actually due to the unusual properties in the “normal” state above the superconducting transition temperature, without understanding which we cannot fully comprehend the nature of high-temperature superconductivity. A schematic phase diagram in Fig. 16 demonstrates the complexities and difficulties we are confronted with. As is known, without doping, cuprates are Mott insulators for the strong electron-electron interactions and in the overdoped regime, cuprates become Fermi liquid, both of which can now be described reasonably well by existing theories. However, in the intermediate regime, for instance, the pseudogap phase, there are many unusual phenomena which are difficult to understand. Previous experimental facts and theoretical models have been discussed in existing reviews^[88–93]. Here, we will present the thermal Hall

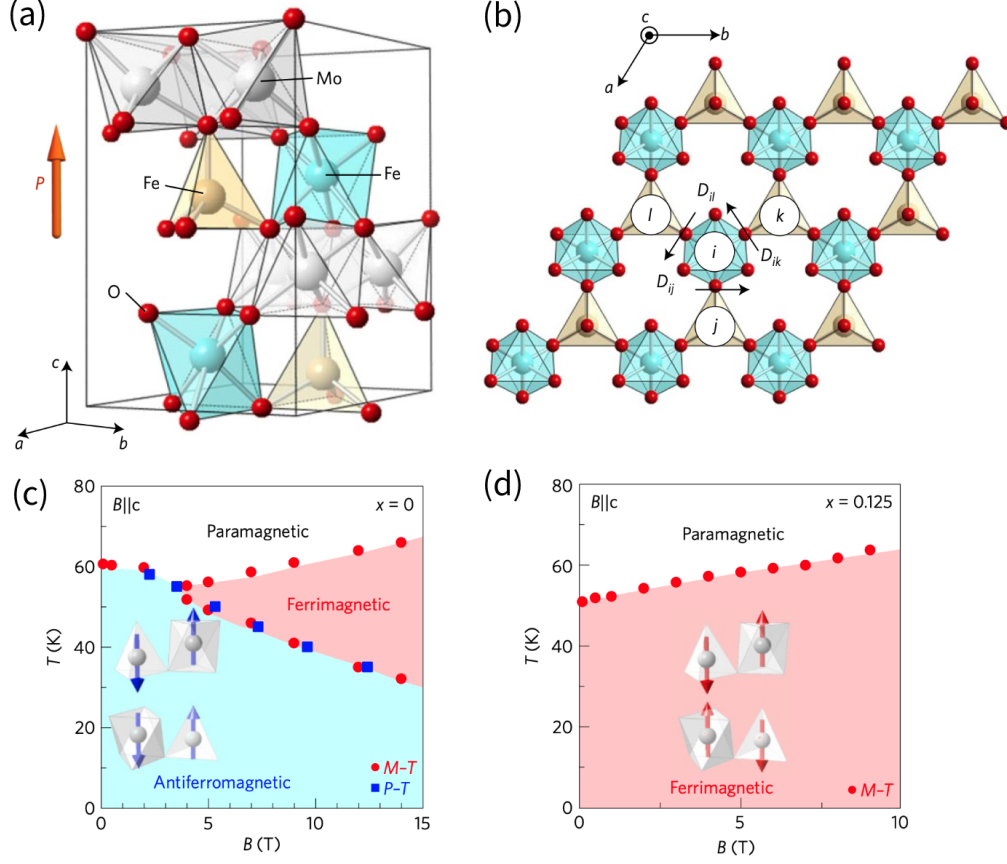


Fig. 14. Crystal structure of $(\text{Fe}_{1-x}\text{Zn}_x)_2\text{Mo}_3\text{O}_8$, side (a) and top (b) view. Magnetic phase diagram for undoped (c) and doped (d) crystals^[87].

transport properties in cuprates^[29,41].

The thermal Hall conductivity in the Cu-O plane in the parent compound La_2CuO_4 and its doped compounds $\text{La}_{1.6-x}\text{Nd}_{0.4}\text{Sr}_x\text{CuO}_4$ (Nd-LSCO), $\text{La}_{1.8-x}\text{Eu}_{0.2}\text{Sr}_x\text{CuO}_4$ (Eu-LSCO), $\text{La}_{2-x}\text{Sr}_x\text{CuO}_4$ (LSCO) is explored^[29], as shown in Fig. 17(b). A large negative κ_{xy} is observed in the normal state, with superconductivity suppressed by the magnetic field and it suddenly changes sign and becomes even larger when the hole doping level $p > p^*$, as shown in Fig. 17(c). The carrier of such a large κ_{xy} is unsettled. First, it cannot be electrons since the parent compound, a Mott insulator can also generate large signals. Second, it cannot be magnons, as κ_{xy} remains even without static magnetism. Excluding other exotic excitations, a plausible guess is phonons. This scenario is then strongly suggested by the isotropy of the thermal Hall conductivity^[41] in the pseudogap phase. However, we believe much more efforts need to be devoted in

order to gain further insights into the mechanism underlying the larger thermal Hall conductivity in cuprate high-temperature superconductors.

III. CONCLUSION AND OUTLOOK

We have surveyed basic knowledge and some experimental facts of THE in strongly correlated electronic systems. The central point is to determine the type of the dominant heat carrier and figure out the microscopic mechanism to generate transverse velocity. The mechanism of magnon Hall effect in DMI systems and phonon Hall effect in SrTiO_3 can now be almost understood. The former furnishes the information that the intrinsic topological properties—nontrivial Berry curvature can generate a κ_{xy} and the latter delivers the message that phonons are able to generate an enhanced thermal Hall signal by skew scattering, which may be a

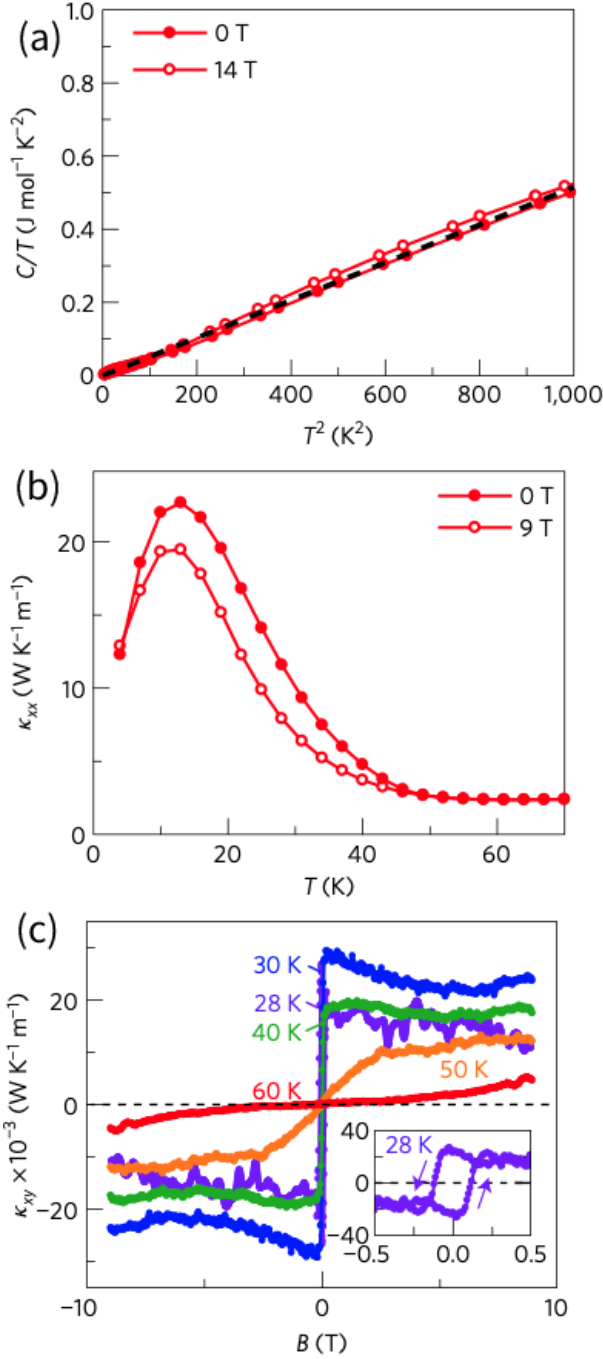


Fig. 15. The specific heat (a), thermal conductivity (b) and thermal Hall conductivity (c) of $(\text{Fe}_{0.875}\text{Zn}_{0.125})_2\text{Mo}_3\text{O}_8$ [87].

hint for the origin of the giant thermal Hall conductivity in multiferroics and pseudogap phase. In multiferroic material $(\text{Fe}_{0.875}\text{Zn}_{0.125})_2\text{Mo}_3\text{O}_8$, the specific heat exhibits a phonon-like behavior and is scarcely affected by the magnetic field. However, κ_{xx} is suppressed by field, inconsistent to phononic scenario. More interest-

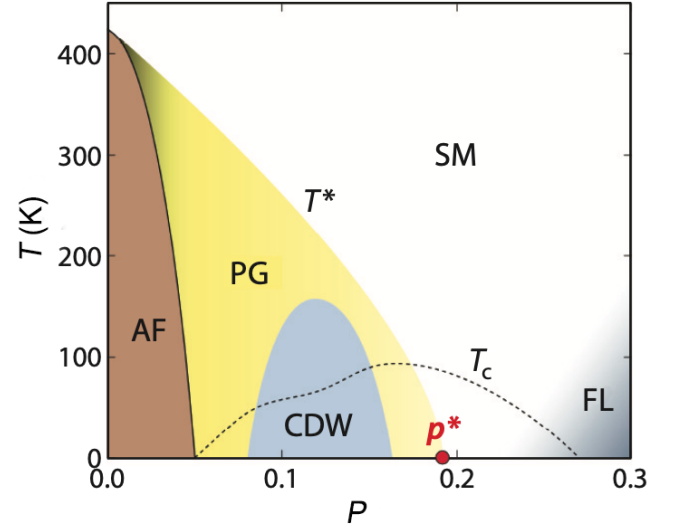


Fig. 16. The phase diagram of hole-doped cuprates [94]. AF, PG, CDW, FL, and SM represent the antiferromagnetic, pseudogap, charge-density-wave, Fermi-liquid, and strange-metal phases, respectively. T^* refers to the temperature of the border of the PG and SM phase. The p^* is the critical concentration separating the PG and SM phase. T_c denotes the superconducting transition temperature.

ingly, under the circumstance where there is no conventional magnon Hall effect, quite large κ_{xy} is observed and it exhibits different qualitative behavior above and under T_N . Since it is known that in multiferroics, spin and lattice couple strongly with each other, it is feasible to ascribe these strange behavior to the strong spin-lattice coupling. In the pseudogap phase in the cuprate high-temperature superconductors, κ_{xy}/T will go down towards negative values at low temperatures. Two important questions should be asked: first, how could the heat carriers (probably phonons) be scattered so strongly in the pseudogap phase and second, what is the difference between phases with $p < p^*$ and $p > p^*$? It seems that both questions point to the mysterious microscopic mechanism of high-temperature superconductivity and as a result, THE may provide another key window for us to understand it. In the quantum spin liquid candidate material $\alpha\text{-RuCl}_3$, origins of the thermal Hall conductivity are highly controversial. More experimental facts are needed to verify different opinions.

Based on the existing theories and experimental facts, some other interesting theories may get involved in the THE. For example, in spirit of the enhanced

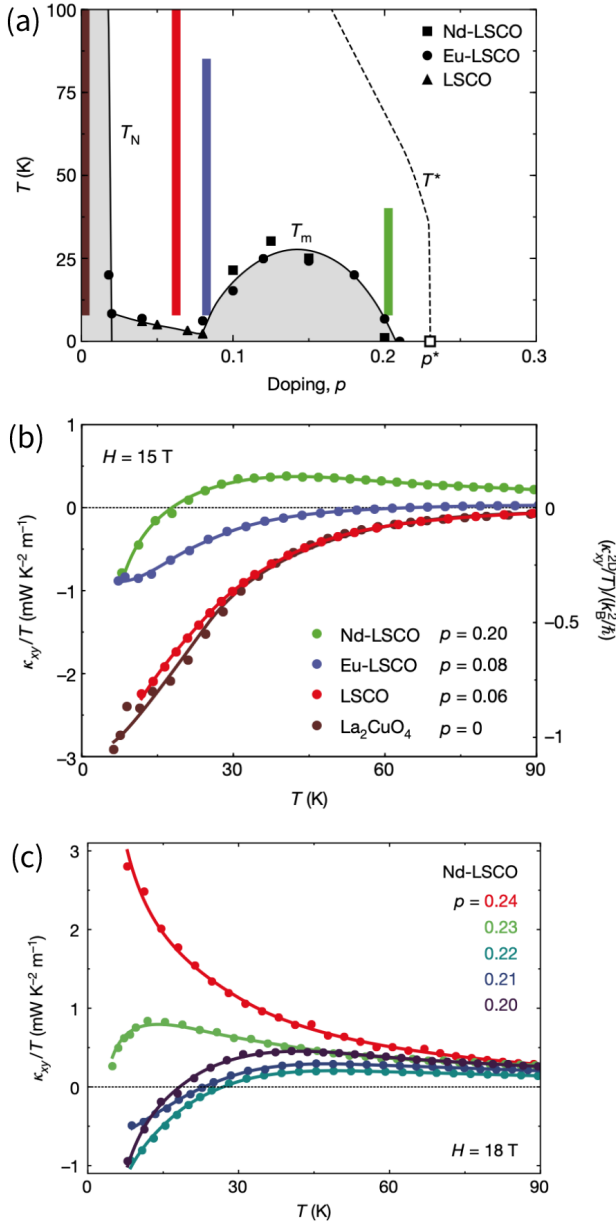


Fig. 17. (a) Phase diagram of cuprates, where short-range incommensurate spin order occurs below T_m . The colored vertical strips indicate the temperature range where κ_{xy}/T decreases towards negative values at low temperatures. (b) Thermal Hall conductivity versus temperature in a field $\mu_0 H = 15$ T. (c) κ_{xy} across the pseudogap critical point p^* [29].

skew scattering, the model for resonant scattering of phonons^[96] are suggested, trying to explain the large THE in La_2CuO_4 , but materials that meet the “resonant conditions” have not yet been found. The chirality of phonons^[41,97,98] is another important factor to affect the Hall response. Chiral phonons are predicted to show Valley phonon Hall effect with strain

gradient^[97], similar to Valley Hall effect^[99]. However, relevant research is still lacking.

Besides specific microscopic models, a generic behavior of thermal Hall conductivity for both fermionic and bosonic systems has been analyzed^[95] with reasonable assumptions, as shown in Fig. 18. It is shown that in a very large temperature range relevant to typical experimental conditions, the thermal Hall conductivity exhibits a universal scaling behavior of the exponential form (e^{-T/T_0}), indicating that there may be a universal framework in the understanding of the THE. Nevertheless, unveiling the mystery beneath the interesting experimental observations is still urgently calling for comprehensive and collaborative work from both experimental and theoretical sides.

The relationship between $|\kappa_{xy}|$ and κ_{xx} is shown in Fig. 19. In DMI systems, such as in $\text{Lu}_2\text{V}_2\text{O}_7$ and $\text{Cu}(1,3\text{-bdc})$, $|\kappa_{xy}|$ scarcely changes with κ_{xx} , which indicates that κ_{xy} is determined by the Berry curvature and is not much influenced by the mean scattering time τ . In the meanwhile, however, the quantum spin ice compound $\text{Tb}_2\text{Ti}_2\text{O}_7$ shows the opposite behavior. Additionally, κ_{xy} in $\text{Fe}_2\text{Mo}_3\text{O}_8$ is quite large,

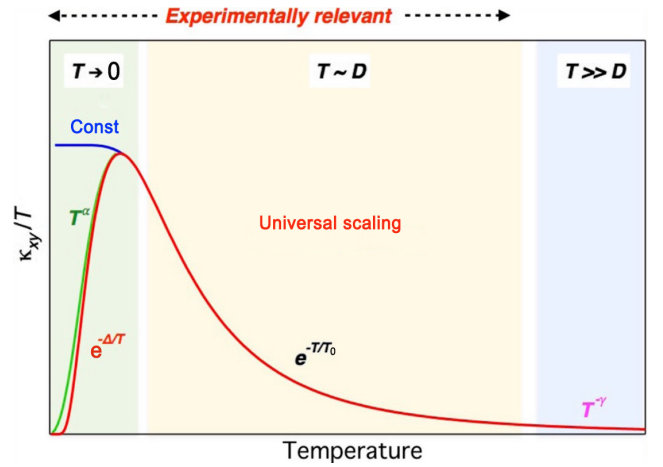


Fig. 18. Sketch of the three temperature regions for the thermal Hall conductivity: the low-temperature region with saturating (const), power-law (T^α), or activation ($e^{-\Delta/T}$) behaviors that reflect different spectral properties of the underlying excitations; the intermediate temperature region with a universal scaling law of the exponential form (e^{-T/T_0}) for $T \sim D$, where D represents the characteristic energy for topologically nontrivial excitations; the high-temperature limit with a $T^{-\gamma}$ scaling, where $\gamma = 1$ for bosons and $\gamma = 3$ for fermions. Only the former two regions are experimentally relevant.^[95]

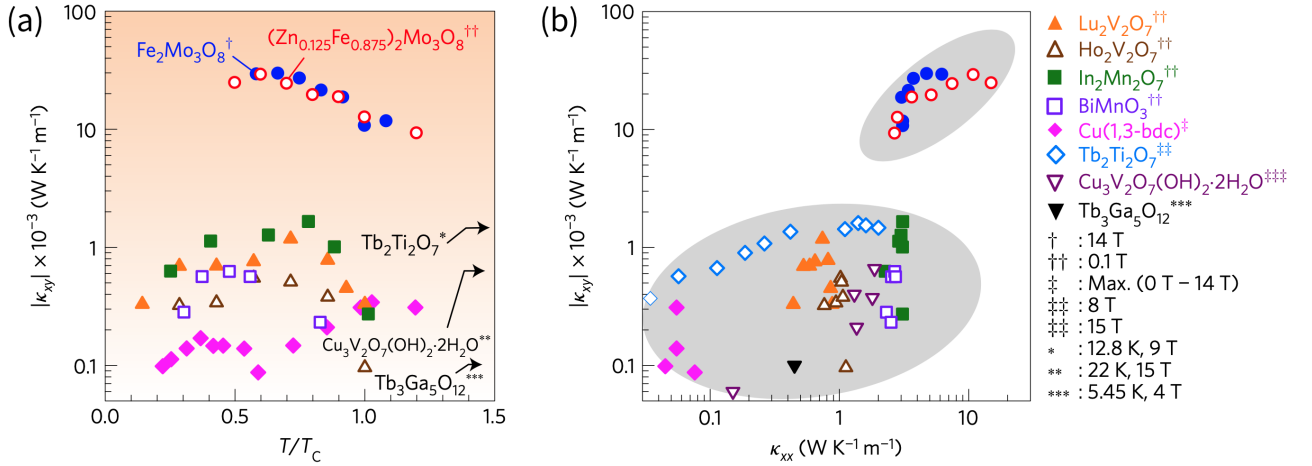


Fig. 19. (a) Thermal Hall conductivity $|\kappa_{xy}|$ as a function of normalized temperature T/T_c (T_c denotes the magnetic phase transition temperature). (b) $|\kappa_{xy}|$ versus κ_{xx} in various insulators^[87].

even one magnitude larger than those in other materials, while its thermal Hall angle is still small, with $|\kappa_{xy}/\kappa_{xx}| \approx 10^{-3}$. This similar result is also found in $\alpha\text{-RuCl}_3$ where different samples show different κ_{xx} and κ_{xy} but the ratios are all in the same magnitude, 1×10^{-3} ^[86], which is considered as evidence for phonon Hall effect. Therefore, this graph can, to some extent, furnish some important information between κ_{xx} and κ_{xy} and it may also help us classify different origins of thermal Hall conductivity efficiently.

The exploration of THE is just in the beginning. THE provides another perspective to unveil the mysteries in strongly correlated electronic materials. The current theories which can explain some phenomena in some systems are still incomplete but are being rapidly developed. With more and more materials with excellent thermal Hall transport properties being discovered and the properties being controlled easily, applications of thermal devices should definitely take a step forward. In addition, THE will help us further understand magnons, phonons as well as their interactions, which can also promote applications in spintronic and magnonic devices.

ACKNOWLEDGMENTS

The work was supported by National Key Projects for Research and Development of China with Grant

No. 2021YFA1400400, the National Natural Science Foundation of China with Grants No. 12225407 and 12074174, China Postdoctoral Science Foundation with Grants No. 2022M711569 and 2022T150315, Jiangsu Province Excellent Postdoctoral Program with Grant No. 20220ZB5, and Fundamental Research Funds for the Central Universities.

REFERENCES

- [1] ANDO T, MATSUMOTO Y, UEMURA Y, Theory of Hall effect in a two-dimensional electron system[J]. J. Phys. Soc. Jpn., 1975, 39: 279.
- [2] ZHANG Y, TAN Y W, STORMER H L, KIM P, Experimental observation of the quantum Hall effect and Berry's phase in graphene[J]. Nature, 2005, 438: 201.
- [3] KLITZING K V, DORDA G, PEPPER M. New method for high-accuracy determination of the fine-structure constant based on quantized Hall resistance[J]. Phys. Rev. Lett., 1980, 45: 494.
- [4] TSUI D C, STORMER H L, GOSSARD A C. Two-dimensional magnetotransport in the extreme quantum limit[J]. Phys. Rev. Lett., 1982, 48: 1559.
- [5] STORMER H L, TSUI D C, GOSSARD A C. The fractional quantum Hall effect[J]. Rev. Mod. Phys., 1999, 71: S298.
- [6] JAIN J K. Theory of the fractional quantum Hall effect[J]. Phys. Rev. B, 1990, 41: 7653.
- [7] THOULESS D J, KOHMOTO M, NIGHTINGALE M P, DEN NIJS M. Quantized hall conductance in a two-

- dimensional periodic potential[J]. Phys. Rev. Lett., 1982, 49: 405.
- [8] HALDANE F D M. Model for a quantum Hall effect without Landau levels: condensed-matter realization of the “parity anomaly”[J]. Phys. Rev. Lett., 1988, 61: 2015.
- [9] KANE C L, MELE E J. Quantum spin Hall effect in graphene[J]. Phys. Rev. Lett., 2005, 95: 226801.
- [10] KANE C L, MELE E J. Z_2 topological order and the quantum spin Hall effect[J]. Phys. Rev. Lett., 2005, 95: 146802.
- [11] FU L, KANE C L. Time reversal polarization and a Z_2 adiabatic spin pump[J]. Phys. Rev. B, 2006, 74: 195312.
- [12] JUNGWIRTH T, NIU Q, MACDONALD A H. Anomalous Hall effect in ferromagnetic semiconductors[J]. Phys. Rev. Lett., 2002, 88: 207208.
- [13] NAGAOSA N, SINOVA J, ONODA S, et al. Anomalous Hall effect[J]. Rev. Mod. Phys., 2010, 82: 1539.
- [14] HALL E. XVIII. on the “rotational coefficient” in nickel and cobalt[J]. Lond. Edinb. Dublin Philos. Mag. J. Sci, 1881, 12: 157.
- [15] KARPLUS R, LUTTINGER J M. Hall effect in ferromagnetics[J]. Phys. Rev., 1954, 95: 1154 .
- [16] HE K, WANG Y, XUE Q K. Quantum anomalous Hall effect[J]. Natl. Sci. Rev., 2014, 1: 38.
- [17] KATSURA H, NAGAOSA N, LEE P A. Theory of the thermal Hall effect in quantum magnets[J]. Phys. Rev. Lett., 2010, 104: 066403.
- [18] QIN T, NIU Q, SHI J. Energy magnetization and the thermal Hall effect[J]. Phys. Rev. Lett., 2011, 107: 236601.
- [19] ZHANG L, REN J, WANG J S, LI B. Topological nature of the phonon Hall effect[J]. Phys. Rev. Lett., 2010, 105: 225901.
- [20] QIN T, ZHOU J, SHI J. Berry curvature and the phonon Hall effect[J]. Phys. Rev. B, 2012, 86: 104305.
- [21] DYAKONOV M I, PEREL V I. Current-induced spin orientation of electrons in semiconductors[J]. Phys. Lett., 1971, A35: 459.
- [22] KATO Y K, MYERS R C, GOSSARD A C, AWSCHALOM D D. Observation of the spin Hall effect in semiconductors[J]. Science, 2004, 306: 1910.
- [23] GORBATYI I N. Spin hall effect in semiconductor structures with spatially inhomogeneous spin relaxation[J]. Semiconductors, 2009, 43: 1002.
- [24] KAPLAN D B. A method for simulating chiral fermions on the lattice[J]. Phys. Lett. B, 1992, 288: 342.
- [25] GOLTERMAN M F L, JANSEN K, KAPLAN D B. Chern-simons currents and chiral fermions on the lattice[J]. Phys. Lett. B, 1993, 301: 219.
- [26] BERNEVIG B A, ZHANG S C. Quantum spin Hall effect[J]. Phys. Rev. Lett., 2006, 96: 106802.
- [27] YOKOI T, MA S, KASAHARA Y, et al. Halfinteger quantized anomalous thermal Hall effect in the Kitaev material α - RuCl_3 [J]. Science, 2021, 373: 568.
- [28] ONOSE Y, IDEUE T, KATSURA H, et al. Observation of the magnon Hall effect[J]. Science, 2010, 329: 297.
- [29] GRISSONNANCHE G, LEGROS A, BADOUX S, et al. Giant thermal Hall conductivity in the pseudogap phase of cuprate superconductors[J]. Nature, 2019, 571: 376.
- [30] DZYALOSHINSKY I. A thermodynamic theory of “weak” ferromagnetism of antiferromagnetics[J]. J. Phys. Chem. Solids, 1958, 4: 241.
- [31] MORIYA T. Anisotropic superexchange interaction and weak ferromagnetism[J]. Phys. Rev., 1960, 120: 91.
- [32] FERT A, LEVY P M. Role of anisotropic exchange interactions in determining the properties of spin-glasses[J]. Phys. Rev. Lett., 1980, 44: 1538.
- [33] IDEUE T, ONOSE Y, KATSURA H, et al. Effect of lattice geometry on magnon Hall effect in ferromagnetic insulators[J]. Phys. Rev. B, 2012, 85: 134411.
- [34] CHISNELL R, HELTON J S, FREEDMAN D E, et al. Topological magnon bands in a kagome lattice ferromagnet[J]. Phys. Rev. Lett., 2015, 115: 147201.
- [35] SHENG L, SHENG D N, TING S C. Theory of the phonon Hall effect in paramagnetic dielectrics[J]. Phys. Rev. Lett., 2006, 96: 155901.
- [36] ZHANG L, YAN Y, WU C Q, WANG J S, LI B. Reversal of thermal rectification in quantum systems[J]. Phys. Rev. B, 2009, 80: 172301.
- [37] KAGAN Y, MAKSIMOV L A. Anomalous Hall effect for the phonon heat conductivity in paramagnetic dielectrics[J]. Phys. Rev. Lett., 2008, 100: 145902.
- [38] AGARWALLA B K, ZHANG L, WANG J S, LI B. Phonon Hall effect in ionic crystals in the presence of static magnetic field[J]. Eur. Phys. J. B, 2011, 81: 197.
- [39] MORI M, SPENCER-SMITH A, SUSHKOV O P, MAEKAWA S. Origin of the phonon Hall effect in rare-earth garnets[J]. Phys. Rev. Lett., 2014, 113: 265901.
- [40] CHEN J Y, KIVELSON S A, SUN X Q. Enhanced thermal Hall effect in nearly ferroelectric insulators[J]. Phys. Rev. Lett., 2020, 124: 167601.
- [41] GRISSONNANCHE G, THÉRIAULT S, GOURGOUT A, et al. Chiral phonons in the pseudogap phase of cuprates[J]. Nat. Phys., 2020, 16: 1108.
- [42] ONSAGER L. Reciprocal relations in irreversible processes. i.[J]. Phys. Rev., 1931, 37: 405.
- [43] CASIMIR H B G. On onsager’s principle of microscopic reversibility[J]. Rev. Mod. Phys., 1945, 17: 343.

- [44] CZAJKA P, GAO T, HIRSCHBERGER M, et al. Oscillations of the thermal conductivity in the spin-liquid state of α - RuCl_3 [J]. *Nat. Phys.*, 2021, 17: 915.
- [45] BOURGEOIS-HOPE P, LALIBERTÉ F, LEFRANÇOIS E, et al. Thermal conductivity of the quantum spin liquid candidate $\text{EtMe}_3\text{Sb}[\text{Pd}(\text{dmit})_2]_2$: no evidence of mobile gapless excitations[J]. *Phys. Rev. X*, 2019, 9: 041051.
- [46] HIRSCHBERGER M, CHISNELL R, LEE Y S, et al. Thermal Hall effect of spin excitations in a kagome magnet[J]. *Phys. Rev. Lett.*, 2015, 115: 106603.
- [47] MATSUMOTO R, MURAKAMI S. Theoretical prediction of a rotating magnon wave packet in ferromagnets[J]. *Phys. Rev. Lett.*, 2011, 106: 197202.
- [48] ATOU T, CHIBA H, OHYAMA K, et al. Structure determination of ferromagnetic perovskite BiMnO_3 [J]. *J. Solid State Chem.*, 1999, 145: 639.
- [49] GOODENOUGH J B. Theory of the role of covalence in the perovskite-type manganites $[\text{La}, \text{M}(\text{II})]\text{MnO}_3$ [J]. *Phys. Rev.*, 1955, 100: 564.
- [50] STROHM C, RIKKEN G L J A, WYDER P. Phenomenological evidence for the phonon Hall effect[J]. *Phys. Rev. Lett.*, 2005, 95: 155901.
- [51] LI X, FAUQUÉ B, ZHU Z, BEHNIA K. Phonon thermal Hall effect in strontium titanate[J]. *Phys. Rev. Lett.*, 2020, 124: 105901.
- [52] BALENTS L. Spin liquids in frustrated magnets[J]. *Nature*, 2010, 464: 199.
- [53] HAN T J, HELTON J S, CHU S. et al. Fractionalized excitations in the spin-liquid state of a kagome-lattice antiferromagnet[J]. *Nature*, 2012, 492: 406.
- [54] NAYAK C, SIMON S H, STERN A, et al. Non-abelian anyons and topological quantum computation[J]. *Rev. Mod. Phys.*, 2008, 80: 1083.
- [55] FIELD B, SIMULA T. Introduction to topological quantum computation with non-Abelian anyons[J]. *Quantum Sci. Technol.*, 2018, 3: 045004.
- [56] ZHU Y. Quantum computing with Z_2 abelian anyon system[J/OL]. *arXiv preprints arXiv:2203.17235*, 2022.
- [57] ANDERSON P W. The resonating valence bond state in La_2CuO_4 and superconductivity[J]. *Science*, 1987, 235: 1196.
- [58] SHIMIZU Y, MIYAGAWA K, KANODA K, et al. Spin liquid state in an organic mott insulator with a triangular lattice[J]. *Phys. Rev. Lett.*, 2003, 91: 107001.
- [59] ITOU T, OYAMADA A, MAEGAWA S, KATO R. Instability of a quantum spin liquid in an organic triangular-lattice antiferromagnet[J]. *Nat. Phys.*, 2010, 6: 673.
- [60] RIBAK A, SILBER I, BAINES C, et al. Gapless excitations in the ground state of $1T-\text{TaS}_2$ [J]. *Phys. Rev. B*, 2017, 96: 195131.
- [61] MA Z, WANG J, DONG Z Y, et al. Spin-glass ground state in a triangular-lattice compound YbZnGaO_4 [J]. *Phys. Rev. Lett.*, 2018, 120: 087201.
- [62] SHEN Y, LI Y D, WALKER H C, et al. Fractionalized excitations in the partially magnetized spin liquid candidate YbMgGaO_4 [J]. *Nat. Commun.*, 2018, 9: 4138.
- [63] FENG Z, LI Z, MENG X, et al. Gapped spin-1/2 spinon excitations in a new kagome quantum spin liquid compound $\text{Cu}_3\text{Zn}(\text{OH})_6\text{FBr}$ [J]. *Chin. Phys. Lett.*, 2017, 34: 077502.
- [64] DING Z F, YANG Y X, ZHANG J, et al. Possible gapless spin liquid in the rare-earth kagome lattice magnet $\text{Tm}_3\text{Sb}_3\text{Zn}_2\text{O}_{14}$ [J]. *Phys. Rev. B*, 2018, 98: 174404.
- [65] OKAMOTO Y, NOHARA M, ARUGA-KATORI H, TAKAGI H. Spin-liquid state in the $S = 1/2$ hyperkagome antiferromagnet $\text{Na}_4\text{Ir}_3\text{O}_8$ [J]. *Phys. Rev. Lett.*, 2007, 99: 137207.
- [66] KOTESWARARAO B, KUMAR R, KHUNTIA P, et al. Magnetic properties and heat capacity of the three-dimensional frustrated $S = 1/2$ antiferromagnet $\text{PbCuTe}_2\text{O}_6$ [J]. *Phys. Rev. B*, 2014, 90: 035141.
- [67] BALZ C, LAKE B, BEUTHER J, et al. et al. Physical realization of a quantum spin liquid based on a complex frustration mechanism[J]. *Nat. Phys.*, 2016, 12: 942.
- [68] O'MALLEY M J, VERWEIJ H, WOODWARD P M. Structure and properties of ordered Li_2IrO_3 and Li_2PtO_3 [J]. *J. Solid State Chem.*, 2008, 181: 1803.
- [69] JACKELI G, KHALIULLIN G. Mott insulators in the strong spin-orbit coupling limit: from heisenberg to a quantum compass and Kitaev models[J]. *Phys. Rev. Lett.*, 2009, 102: 017205.
- [70] KIMCHI I, COLDEA R, VISHWANATH A. Unified theory of spiral magnetism in the harmonichoneycomb iridates α , β , and γ Li_2IrO_3 [J]. *Phys. Rev. B*, 2015, 91: 245134.
- [71] BANERJEE A, BRIDGES C A, YAN J Q. et al. Proximate Kitaev quantum spin liquid behaviour in a honeycomb magnet[J]. *Nat. Mater.*, 2016, 15: 733.
- [72] SANDILANDS L J, TIAN Y, PLUMB K W, et al. Scattering continuum and possible fractionalized excitations in α - RuCl_3 [J]. *Phys. Rev. Lett.*, 2015, 114: 147201.
- [73] KIM B J, JIN H, MOON S J, et al. Novel $J_{\text{eff}} = 1/2$ mott state induced by relativistic spin-orbit coupling in Sr_2IrO_4 [J]. *Phys. Rev. Lett.*, 2008, 101: 076402.
- [74] RAN K J, WANG J H, WEN J S. A new route to quantum spin liquids: material realization of the Kitaev model[J]. *Physics*, 2021, 50: 443.
- [75] WANG W, DONG Z Y, YU S L, LI J X. Theoreti-

- cal investigation of magnetic dynamics in α -RuCl₃[J]. Phys. Rev. B, 2017, 96: 115103.
- [76] KIM H S, KEE H Y. Crystal structure and magnetism in α -RuCl₃ : An *ab initio* study[J]. Phys. Rev. B, 2016, 93: 155143.
- [77] CAO H B, BANERJEE A, YAN J Q, et al. Low-temperature crystal and magnetic structure of α -RuCl₃[J]. Phys. Rev. B, 2016, 93: 134423.
- [78] ITAEV A. Anyons in an exactly solved model and beyond[J]. Ann. Phys., 2006, 321: 2.
- [79] BANERJEE A, YAN J, KNOLLE J, et al. Neutron scattering in the proximate quantum spin liquid α -RuCl₃, Science, 2017 356: 1055.
- [80] DO S H, PARK S Y, YOSHITAKE J, et al. Majorana fermions in the Kitaev quantum spin system α -RuCl₃[J]. Nat. Phys., 2017, 13: 1079.
- [81] KASAHARA Y, OHNISHI T, MIZUKAMI Y, et al. quantization and half-integer thermal quantum Hall effect in a Kitaev spin liquid, Nature, 2018, 559: 227.
- [82] READ N. GREEN E. Paired states of fermions in two dimensions with breaking of parity and timereversal symmetries and the fractional quantum Hall effect[J]. Phys. Rev. B, 2000, 61: 10267.
- [83] KASAHARA Y, SUGII K, OHNISHI T, et al. Unusual Thermal Hall Effect in a Kitaev Spin Liquid Candidate α -RuCl₃[J]. Phys. Rev. Lett., 2018, 120: 217205.
- [84] BRUIN J A N, R. CLAUS R, MATSUMOTO Y. et al. Robustness of the thermal Hall effect close to half-quantization in α -RuCl₃[J]. Nat. Phys., 2022, 18: 401.
- [85] HENTRICH R, WOLTER A U B, ZOTOS X, et al. Unusual phonon heat transport in α -RuCl₃ : strong spin-phonon scattering and field-induced spin gap[J]. Phys. Rev. Lett., 2018, 120: 117204.
- [86] LEFRANÇOIS É, GRISSONNANCHE G , BAGLO J, et al. Evidence of a phonon Hall effect in the kitaev spin liquid candidate α -RuCl₃[J]. Phys. Rev. X, 2022, 12: 021025.
- [87] IDEUE T, KURUMAJI T, ISHIWATA S, TOKURA Y. Giant thermal Hall effect in multiferroics[J]. Nat. Mater., 2017, 16: 797.
- [88] SADOVSKII M V. Pseudogap in high-temperature superconductors[J]. Phys.-Usp., 2001, 44: 515.
- [89] TIMUSK T, STATT B. The pseudogap in high-temperature superconductors: An experimental survey[J]. Rep. Prog. Phys., 1999, 62: 61.
- [90] JEZEQUEL G, THOMAS J, POLLINI I. Experimental band structure of semimetal bismuth[J]. Phys. Rev. B, 1997, 56: 6620.
- [91] GUSYNIN V P, LOKTEV V M, SHOYKOVY I A. On the superconductivity of 2d system with arbitrary carrier density in external magnetic field[J/OL]. arXiv preprints arXiv.cond-mat/9506102, 1995.
- [92] GESHKENBEIN V B, IOFFE L B, LARKIN A I. Superconductivity in a system with preformed pairs[J]. Phys. Rev. B, 1997, 55: 3173.
- [93] MALY J, JANKÓ B, LEVIN K. Superconductivity from a pseudogapped normal state: a mode coupling approach to precursor superconductivity[J]. Phys. Rev. B, 1999, 59: 1354.
- [94] PROUST C, TAILLEFER L. The remarkable underlying ground states of cuprate superconductors[J]. Annu. Rev. Condens. Matter Phys., 2019, 10: 409.
- [95] YANG Y F, ZHANG G M, ZHANG F C. Universal behavior of the thermal Hall conductivity[J]. Phys. Rev. Lett., 2020, 124: 186602.
- [96] SUN X Q, CHEN J Y, KIVELSON S A. Large extrinsic phonon thermal Hall effect from resonant scattering 10.48550/ARXIV.2109.12117, 2021.
- [97] ZHANG L. NIU Q. Chiral phonons at high-symmetry points in monolayer hexagonal lattices[J]. Phys. Rev. Lett., 2015, 115: 115502.
- [98] ZHU H, YI J, LI M Y, et al. Observation of chiral phonons[J]. Science, 2018, 359: 579.
- [99] XIAO D, YAO W, NIU Q. Valley-contrasting physics in graphene: magnetic moment and topological transport[J]. Phys. Rev. Lett., 2007, 99: 236809.

强关联材料霍尔热导率实验测量综述

徐 豪¹, 承舒凡¹, 鲍 嵩^{1*}, 温锦生^{1,2†}

1. 南京大学物理学院, 固体微结构物理国家重点实验室, 南京 210093

2. 人工微结构科学与技术协同创新中心, 南京大学, 南京 210093

摘要: 在材料中输入热流并在垂直于热流的方向上施加磁场时, 热载流子将可能被磁场偏转, 获得横向速度, 从而导致材料在横向出现一个温度梯度。这种效应被称为热霍尔效应 (THE)。与电霍尔效应类似, 热霍尔效应被预言将在一些拥有非平庸贝利曲率的材料中出现, 因此它可以揭示材料的拓扑性质。然而, 热霍尔效应并不像电霍尔一样, 只局限于载流子带电的体系; 相反, 任何种类的准粒子都可以导热。因此, 热霍尔效应也可以用来探索强关联电子体系材料 (尤其是绝缘体) 的奇异性质。因此, 热霍尔效应更具有普适性, 并日益成为探测电中性激发, 如声子和磁振子的强有力手段。不仅如此, 有如手性声子这样超越一般非平庸贝利曲率图像的因素仍可导致热霍尔效应; 探查其中的热霍尔效应将为理解材料中复杂的微观机理指明方向。但是, 热信号比电信号要微弱得多。尤其是测量热霍尔效应, 往往要在较大背景噪音中提取微弱的有效信号, 这使霍尔热导的测量极具挑战性。但是得益于科研工作者大量的努力, 该领域在近几年发展迅速, 得到了许多十分有趣的结果。在本文中, 我们将简要总结现有的一些令人兴奋的在霍尔热导率测量方面的成果, 指出尚未解决的问题, 并提出未来可能的方向。

关键词: 热霍尔效应; 拓扑; 量子自旋液体; 多铁材料; 赝能隙相

* E-mail: songbao@nju.edu.cn

† E-mail: jwen@nju.edu.cn